SPRINGER BRIEFS IN ELECTRICAL AND COMPUTER ENGINEERING · COMPUTATIONAL ELECTROMAGNETICS

Shiv Narayan
K.M. Divya
V. Krushna Kanth

FDTD Modeling of EM Field Inside Microwave Cavities

Springer

SpringerBriefs in Electrical and Computer Engineering

Computational Electromagnetics

More information about this series at http://www.springer.com/series/13885

Shiv Narayan · K.M. Divya · V. Krushna Kanth

FDTD Modeling of EM Field Inside Microwave Cavities

Springer

Shiv Narayan
Centre for Electromagnetics
CSIR-National Aerospace Laboratories
Bangalore, Karnataka
India

V. Krushna Kanth
Centre for Electromagnetics
CSIR-National Aerospace Laboratories
Bangalore, Karnataka
India

K.M. Divya
Centre for Electromagnetics
CSIR-National Aerospace Laboratories
Bangalore, Karnataka
India

ISSN 2191-8112 ISSN 2191-8120 (electronic)
SpringerBriefs in Electrical and Computer Engineering
ISSN 2365-6239 ISSN 2365-6247 (electronic)
SpringerBriefs in Computational Electromagnetics
ISBN 978-981-10-3414-5 ISBN 978-981-10-3415-2 (eBook)
DOI 10.1007/978-981-10-3415-2

Library of Congress Control Number: 2016960283

Printed on acid-free paper

This Springer imprint is published by Springer Nature
The registered company is Springer Nature Singapore Pte Ltd.
The registered company address is: 152 Beach Road, #22-06/08 Gateway East, Singapore 189721, Singapore

Dedicated to Late Dr. Rakesh Mohan Jha

Preface

The microwave cavity resonators have been widely used in various equipment such as microwave ovens, radars, and satellite communications since past few decades. Recently, it is used in autoclave to achieve desire temperature distribution inside the autoclave. In order to maintain the appropriate temperature inside the autoclave/oven, it is necessary to estimate field distribution inside their cavity accurately.

In view of this, the EM analysis of field distribution inside some microwave cavities is presented in this book based on three-dimensional FDTD method. For the analysis, basically two types of closed microwave cavities are considered: (i) domestic rectangular microwave oven and (ii) industrial hybrid-cylindrical microwave autoclave. In these devices, the EM field distribution inside their cavity is estimated in *xy*-, *yz*-, and *zx*-plane. Further, the field distribution inside autoclave cavity is studied in the presence of cubic and cylindrical sample of composite material to show its capability to cure the aerospace components and materials.

This brief is organized as follows: Section 1 deals with the introduction about the work, and Sect. 2 describes the basic theory of FDTD method and its implementation. In Sect. 3, the EM field distribution inside domestic microwave oven is discussed. The modeling of curved microwave cavities including analysis of hybrid-autoclave is carried out in Sect. 4. Finally, Sect. 5 draws the conclusions of the work carried out in the book.

Bangalore, India

Shiv Narayan
K.M. Divya
V. Krushna Kanth

Acknowledgements

We would like to thank Mr. Shyam Chetty, Director, CSIR-National Aerospace Laboratories, Bangalore, for the permission to write this SpringerBrief.

We would like to express our sincere thanks to Dr. R. U. Nair, Head, Centre for Electromagnetics, for his valuable technical support and providing fruitful environment at CEM. We would also like to acknowledge valuable suggestions from our colleagues at the Centre for Electromagnetics, Dr. Hema Singh, Dr. Balamati Choudhury, and Mr. K.S. Venu during the course of writing this book. We express our sincere thanks to Ms. Sangeetha B., Ms. Divya S., and Ms. Sai Samhitha, the project staff at the Centre for Electromagnetics, for their consistent support during the preparation of this book.

But for the concerted support and encouragement of editorial team of Springer India Private Limited it would not have been possible to bring out this book within such a short span of time. We very much appreciate the continued support by Swati Meherishi, Kamiya Khattar, and Aparajita Singh, toward bringing out this brief.

Contents

Abbreviations

AC	Alternative current
DC	Direct current
EM	Electromagnetics
FDTD	Finite difference time domain
HIS	High impedance surfaces
ORBC	Outer radiation boundary condition
PEC	Perfect electric conductor
PML	Perfectly matched layer
UAVs	Unmanned air vehicles

Symbols

δ	Magnetic resistivity
ε	Electric permittivity
ε_r	Relative permittivity
λ	Free-space wavelength
μ	Magnetic permeability
σ_e	Electric conductivity
Δt	Time step
Δx, Δy, Δz	Lattice space increment in *x-*, *y-*, and *z*-axis
$C_{\max}$	Maximum EM wave velocity
D_z	Electric field density
E	Electric field
E_{x_inc}	Electric field component of incident wave
H	Magnetic field
H_{z_inc}	Magnetic field component of incident wave
$\tan\delta_e$	Electric loss tangent

List of Figures

List of Table

FDTD Modeling of EM Field Inside Microwave Cavities

1 Introduction

A microwave cavity is a closed metallic structure that confines electromagnetic fields in the microwave region. The closed structure is filled with either air or dielectric. As cavity is excited with microwave source (e.g., magnetron and klystron), EM wave propagates inside the cavity and bounces back and forth between the walls of the cavity resulting in the formation of standing wave inside the cavity (Liao 1995). A microwave cavity is similar to a circuit resonator with low loss and high-quality factor. There are different types of cavity resonators found in practice such as rectangular cavity resonator, circular cavity resonator, and reentrant cavity resonator. These resonators are used in the microwave ovens, radars, and satellite communication systems.

A microwave oven is essentially a rectangular cavity with a turntable, a microwave source, and a control system. The AC power supply is transformed to DC for driving the magnetron source, which generates microwave signal at 2.45 GHz. In general, microwave oven is used as home appliances. If the door of the oven which serves to secure the food item within the cavity is opened during the operation, the safety switch automatically stops the power flow to the magnetron. However, there is a microwave leakage through the gap between the door and the oven cavity, even when the oven door is closed. The irradiated waves from the chamber to the external environment include various higher order modes because of the complexities of the oven structure (Kusama et al. 2003). This leakage affects the wireless communications in indoor environment aircraft cabin at 2.45 GHz. Thus, it is essential to study the field distribution inside the oven cavity and RF leakage radiation from the door.

Recently, microwave oven is used to cure and sterilize materials and components at different temperatures employed for aerospace and medical sectors, etc. (Samuel 1995). Such kind of oven is called as *microwave autoclave*. Generally, autoclave is excited with multiple magnetron sources to control the field distribution and hence

S. Narayan et al., *FDTD Modeling of EM Field Inside Microwave Cavities*,
SpringerBriefs in Computational Electromagnetics,
DOI 10.1007/978-981-10-3415-2_1

temperature distribution inside the autoclave cavity. It is essential to study the EM (electromagnetic) field distribution to determine the temperature distribution inside autoclave cavity. In order to analyze EM field distribution inside the closed microwave cavity (e.g., microwave oven and autoclave), several methods have been proposed in the open literature. Initially, equivalent transmission line method was proposed to determine the field distribution inside the domestic microwave oven cavity (Watanabe et al. 1978). Further, full-wave method approaches were presented to analyze the EM field distribution inside the arbitrary-shaped and complex microwave oven (Pourcq 1985; Jia and Jolly 1992; Dev et al. 2010).

This book deals with the EM analysis of various closed microwave cavities such as microwave oven and autoclave of normal as well as hybrid shaped. The three-dimensional *finite difference time domain* (FDTD) method is used for the analysis as it is capable of handling closed microwave cavity problems in the presence of complex materials and components. In this endeavor, EM field distribution inside cavity is studied in different plane for (i) domestic microwave oven and (ii) hybrid-cylindrical microwave autoclave. The details of the work are discussed in the following sections.

2 Finite Difference Time Domain Method

The electromagnetic FDTD algorithm was first introduced by Yee in 1966. The algorithm was then modified, refined, and used by many researchers in different areas of electromagnetics. This is a computationally efficient method of directly solving the Maxwell's time-dependent curl equations or their equivalent integral equations using the finite difference technique. Since it is a time domain method, the solutions can cover a wide frequency range with a single simulation run (Rao 1999). This method comes in category of *resonance region* techniques, i.e., ones in which the characteristic dimensions of domain of interest are somewhere on the order of wavelength in size.

The FDTD method belongs to the general class of grid-based differential time domain numerical modeling methods. In this extensively computer-based numerical method, the continuous distribution of electromagnetic fields in a finite volume of space is sampled at distinct points in a space and time lattice, which is called as a *leap-frog* manner. The electromagnetic wave propagation, scattering, and penetration phenomena are modeled in a self-consistent manner by marching in time step, and repeatedly implementing the finite difference numerical analog of Maxwell's equations at each spatial lattice point. This approach basically results in a simulation of the actual coupled EM field full-wave solution by the sampled data, propagating in a data space stored in a computer. The space and time sampling increments are selected to avoid aliasing of the continuous field distribution and to guarantee stability of the time-marching algorithm. The time marching will be completed when the desired time or steady-state field behavior is observed.

An important application of the latter is the sinusoidal steady state which eventually results for a continuous sinusoidal incident excitation (Rao 1999).

2.1 Maxwell's Curl Equations

The FDTD formulation basically initiates from the time domain Maxwell's curl equations. Consider a source-free region and its electromagnetic (EM) parameters are independent of time. The differential time domain Maxwell's equations in a linear isotropic and frequency-independent medium are given as follows:

$$\frac{\partial H}{\partial t} = -\frac{1}{\mu}\nabla \times E - \frac{\delta}{\mu}H \tag{1}$$

$$\frac{\partial E}{\partial t} = -\frac{1}{\varepsilon}\nabla \times H - \frac{\sigma_e}{\varepsilon}E \tag{2}$$

where E is the electric field, H is the magnetic field, ε is the electric permittivity, σ_e is the electric conductivity, and μ is the magnetic permeability. δ is the magnetic resistivity which is included here to account for any magnetic loss and to get symmetric equations.

Equations (1) and (2) can be expressed as six coupled scalar equations in the Cartesian coordinate system (x, y, z) as given (Yee 1966):

$$\frac{\partial H_x}{\partial t} = \frac{1}{\mu}\left[\frac{\partial E_y}{\partial z} - \frac{\partial E_z}{\partial y} - \delta H_x\right] \tag{3}$$

$$\frac{\partial H_y}{\partial t} = \frac{1}{\mu}\left[\frac{\partial E_z}{\partial x} - \frac{\partial E_x}{\partial z} - \delta H_y\right] \tag{4}$$

$$\frac{\partial H_z}{\partial t} = \frac{1}{\mu}\left[\frac{\partial E_x}{\partial z} - \frac{\partial E_y}{\partial y} - \delta H_z\right] \tag{5}$$

$$\frac{\partial E_x}{\partial t} = \frac{1}{\varepsilon}\left[\frac{\partial H_z}{\partial y} - \frac{\partial H_y}{\partial z} - \sigma_e E_x\right] \tag{6}$$

$$\frac{\partial E_y}{\partial t} = \frac{1}{\varepsilon}\left[\frac{\partial H_x}{\partial z} - \frac{\partial H_z}{\partial x} - \sigma_e E_y\right] \tag{7}$$

$$\frac{\partial E_z}{\partial t} = \frac{1}{\varepsilon}\left[\frac{\partial H_y}{\partial x} - \frac{\partial H_x}{\partial y} - \sigma_e E_z\right] \tag{8}$$

The above six partial differential equations starting from (3) to (8) form the building block for FDTD algorithm.

2.2 Yee's Algorithm

The FDTD algorithm proposed by Yee (1966) employs the second-order *central differences*. The algorithm can be summarized as follows:

1. Replace all the derivatives in the Ampere's and Faraday's laws with finite differences. Discretize the space and time so that the electric and magnetic fields are staggered in both space and time.
2. Solve the resulting difference equations to obtain "update equations" that express the (unknown) future fields in terms of (known) past fields.
3. Evaluate the magnetic fields one time step into the future so they are known and effectively they become past fields.
4. Evaluate the electric fields one time step into the future so they are known and effectively they become past fields.
5. Repeat the previous two steps until the fields have been obtained over the required duration (Schneider 2010).

The system of six coupled partial differential equations of Eqs. (3) through (8) forms the basis of the FDTD algorithm for electromagnetic radiation, interference, and interaction with three-dimensional (3-D) objects. The Yee FDTD algorithm is applied on a staggered grid as shown in Fig. 1, which centers its $\vec{E}$ and $\vec{H}$ components in three-dimensional space in such a way that every $\vec{E}$ component is surrounded by four circulating $\vec{H}$ components and every $\vec{H}$ component is surrounded by four circulating $\vec{E}$ components (Taflove and Hagness 2005).

The Cartesian components of the electric field are the unknowns at first grid and the Cartesian components of the magnetic field are the unknowns at the second grid offset from the first by a half-cell distance in each Cartesian direction as shown in Fig. 1. A space point in a rectangular coordinate system is denoted as

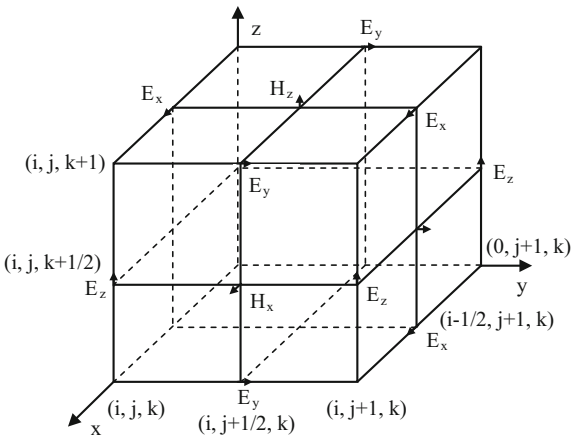

Fig. 1 Yee cell geometry (after Yee 1966)

$$(i,j,k) = (i\Delta x, j\Delta y, k\Delta z) \tag{9}$$

and a function of space and time in rectangular grid is defined as

$$F^n(i,j,k) = F(i\Delta x, j\Delta y, k\Delta z, n\Delta t) \tag{10}$$

where Δx,Δy, and Δz are the lattice space increments in the x-, y-, and z-directions, respectively. Δt is the time increment and i, j, k, and n are the integers. This is known as centered finite difference with second-order accuracy. A space derivative can be expressed as follows:

$$\frac{\partial F^n(i,j,k)}{\partial x} = \frac{F^n(i+1/2,j,k) - F^n(i-1/2,j,k)}{\Delta x} \tag{11}$$

Similarly, the time derivative can be expressed in the same manner as

$$\frac{\partial F^n(i,j,k)}{\partial t} = \frac{F^{n+1/2}(i,j,k) - F^{n-1/2}(i,j,k)}{\Delta t} \tag{12}$$

To achieve the accuracy of Eq. (12), the electric field and the magnetic field values on the two grids are evaluated at alternate half time steps, that is in the *leap-frog manner* (Hussein and Sebak 1996). Substituting these expressions in equations from Eqs. (3) to (8) results in a system of six difference equations. The samples of FDTD expressions for an electric and a magnetic field component are expressed as

$$E_z^{n+1/2}(i,j,k+1/2) = E_z^{n-1/2}(i,j,k+1/2) + \frac{\Delta t}{\Delta x\sqrt{\varepsilon_0\mu_0}} \begin{pmatrix} H_y^n(i+1/2,j,k+1/2) - \\ H_y^n(i-1/2,j,k+1/2) - \\ H_x^n(i,j-1/2,k+1/2) + \\ H_x^n(i,j+1/2,k+1/2) \end{pmatrix} \tag{13}$$

$$H_z^{n+1}(i+1/2,j+1/2,k) = H_z^n(i+1/2,j+1/2,k) - \frac{\Delta t}{\Delta x\sqrt{\varepsilon_0\mu_0}} \begin{pmatrix} E_y^{n+1/2}(i+1,j+1/2,k) - \\ E_y^{n+1/2}(i,j+1/2,k) - \\ E_x^{n+1/2}(i+1/2,j+1,k) + \\ E_x^{n+1/2}(i+1/2,j,k) \end{pmatrix} \tag{14}$$

Similarly, the other components of the electric and the magnetic fields can be obtained.

2.3 Implementation of FDTD Method

In order to apply FDTD method, a computational domain is first established, which is simply a physical region to perform the simulation. The E and H fields are then

determined at every point in space within the computational domain. The material of each cell within the computational domain must be specified which may be either free-space (air) or metal or dielectric. In the computational domain, a material is specified by its permeability, permittivity, and conductivity. A source is specified soon after defining the computational domain and the grid materials. The selection of source type depends on the applications. Some common sources are impinging plane wave, current in a wire, and applied electric field. Since the E and H fields are determined directly in the simulation, the output will be the E or H field at a point or a series of points within the computational domain.

In order to achieve the stability of the time-stepping algorithm of simulation, the space cell size and the time stepping should be considered carefully. The choice of a cell size is critical in applying FDTD. It is required to ensure two points at the time of defining the cell size: (i) It must be small enough to permit accurate results at the higher frequency of interest, and (ii) cell must be large enough to keep computational requirements manageable. In the simulation, the cell size is directly affected by the considered material. For instance, smaller cell size will be required for material with higher permittivity and shorter wavelength at a given frequency. The fundamental constraint for the cell size is that it must be much smaller than the smallest wavelength for which accurate results are desired. In general, at least ten cells per wavelength (i.e., cell size $\sim\lambda/10$) are required in the FDTD simulation for accuracy.

Once the cell size is determined, the maximum size of the time step Δt follows immediately. To insure the stability of the time-stepping algorithm, Δt is chosen to satisfy *Courant inequality*, given as

$$\Delta t \leq \frac{1}{c_{\max}\left[\frac{1}{\Delta x^2}+\frac{1}{\Delta y^2}+\frac{1}{\Delta z^2}\right]^{1/2}} \tag{15}$$

where $c_{\max}$ is the maximum EM wave phase velocity in the medium and is expressed as

$$c_{\max} = \frac{1}{\sqrt{\mu\varepsilon}} \tag{16}$$

For several applications, the modeled structure is situated in free space, such as scatterer and radiating antennas. In such cases, radiated field propagates into boundless space. The usual measures involve the application of an *outer radiation boundary condition* (ORBC) to absorb the scattered or radiated fields reaching at the outmost boundary. There are several schemes to define such boundary. A popular and easily applied ORBC, which is commonly known as *Mur absorbing boundary*, or more particularly the first or second *Mur boundary*, depending on the order of approximation used to determine the field on the boundary (Hussein and Sebak 1996). However, Mur's second-order ABC causes the generation of large spurious wave components in the computational domain when applied to a

boundary having dielectric discontinuity. This is due to the fact that in practice the electromagnetic wave has different velocity in the media with different permittivity. In contrast to this, Mur's second-order ABC assumes all associated E-field components to have similar permittivity and velocity at the boundary between two dielectrics, which is indeed not true. To accomplish such problem, material ABC's called Berenger's perfectly matched layer (1994), is constructed so that fields are dampened as they propagate into the absorbing medium. In this brief, Berenger's PML boundary has been applied to solve the oven as well as autoclave problems.

3 Analysis of EM Field Distribution Inside the Microwave Oven

In the present work, the EM analysis of field distribution inside the domestic microwave oven is carried out using 3D FDTD method. The schematic of a typical LG microwave oven (350 mm × 350 mm × 220 mm) is shown in Fig. 2, where the oven mainly consists of a rectangular cavity which is excited by a TE_{10} mode of plane wave with maximum amplitude of 0.3 V/m, through a rectangular waveguide as given below,

$$E_{z\,inc} = 0.3\sin(2\pi f \cdot \Delta t \cdot T) \tag{17}$$

where f is the frequency of operation and Δt is the time step. This plane wave propagates inside the oven cavity and reflects back and forth from the cavity walls resulting in the formation of the standing wave inside the cavity.

A turntable is employed to generate a time-averaged uniform microwave field to achieve uniform heating within the cavity, which is desirable for cooking. The proposed cavity has a door in the front, shown a bit apart. In order to study the EM

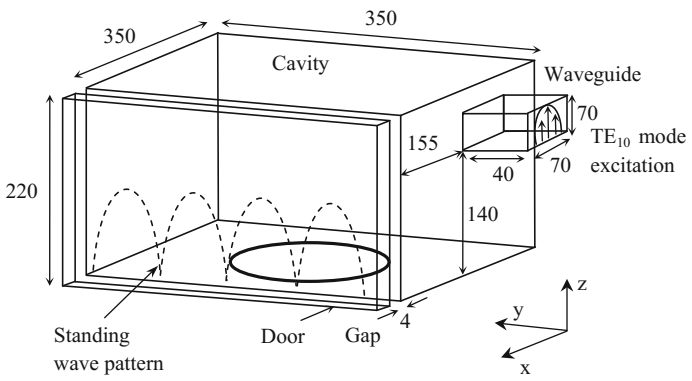

Fig. 2 Schematic of the microwave oven. All dimensions in mm

leakage from the oven, the gap between the door and the cavity is considered to be 4 mm, which seems to be large as compared to practical gap (2 mm). This much gap has been taken to make its FDTD modeling more accurate since the cell size is taken to be $\Delta x = \Delta y = \Delta z = 2$ mm. According to FDTD method, the whole space of EM analysis is divided into multiple small lattices, and electrical constants are assigned to each lattice unit. The perfect electric conductor (PEC) boundary is applied to the metal surfaces and perfectly matched layer (PML) boundary is applied to the whole analysis structure as absorbing boundary.

3.1 RF Leakage Radiation

The EM analysis of RF leakage from the microwave oven is investigated using 3D FDTD method. The oven structure is excited by a TE_{10} mode plane wave through the rectangular waveguide as mentioned above. The standing waves are thus formed inside the cavity as shown in Fig. 3. The power leaking from the upper part of the oven door is computed as shown in Fig. 4, where the magnitude of the total electric field E_{tot} is shown. Further, the E_{tot} component of electric field leaking around the oven door is computed as shown in Fig. 5. It is observed that the upper part of the door acts as the most probable leakage edge. It is also found that the power leaking around the door is composed of mixed modes.

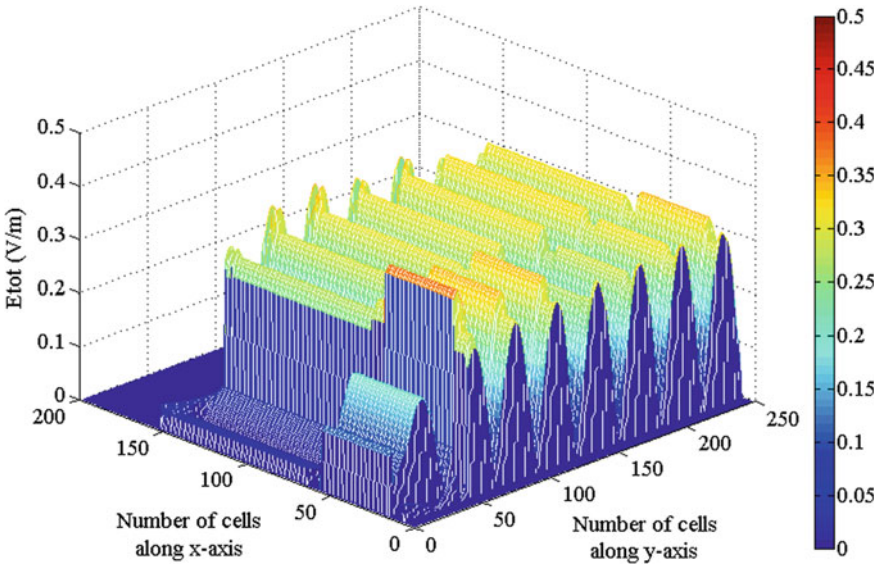

Fig. 3 Electric field standing wave pattern inside the oven cavity

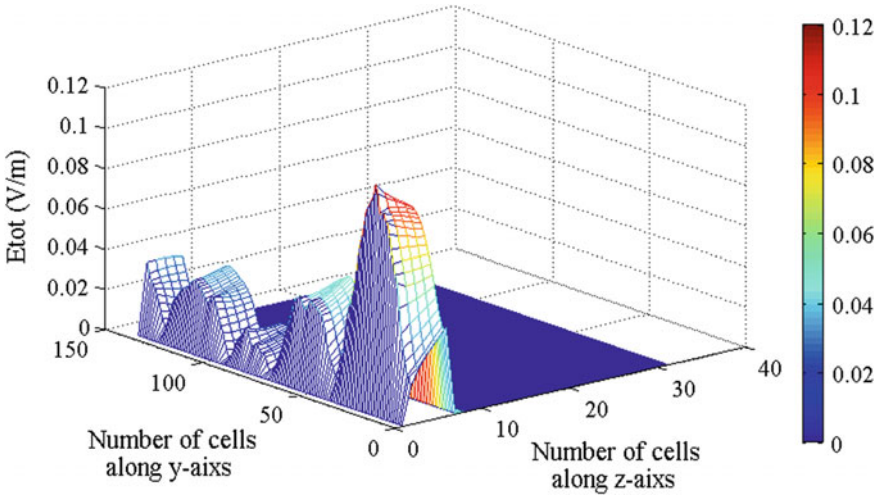

Fig. 4 Leakage of electric field at the *upper part* of the door

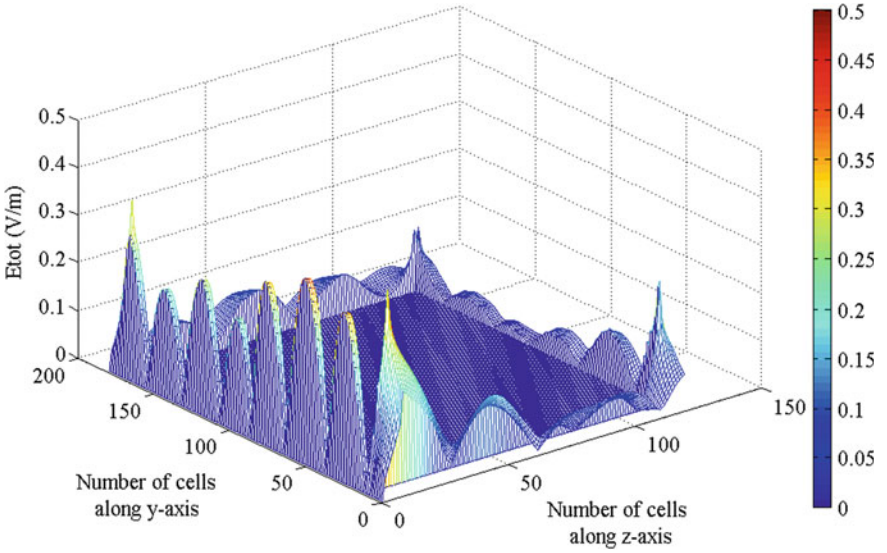

Fig. 5 Leakage of electric field around the door of the oven

3.2 EM Field Distribution Inside the Oven Cavity

The EM field distribution inside the microwave oven is estimated in *xy*-, *yz*-, and *zx*-planes of cavity using three-dimensional FDTD method. Here, the gap between the door and the oven cavity has not been considered. This may be noted that in the above-mentioned planes, magnitude of the total electric field is computed in the unit of V/m and then normalized with the maximum field value in the corresponding plane. Figures 6, 7, 8, 9, 10, 11, 12, 13, 14, and 15 represent the magnitude of total

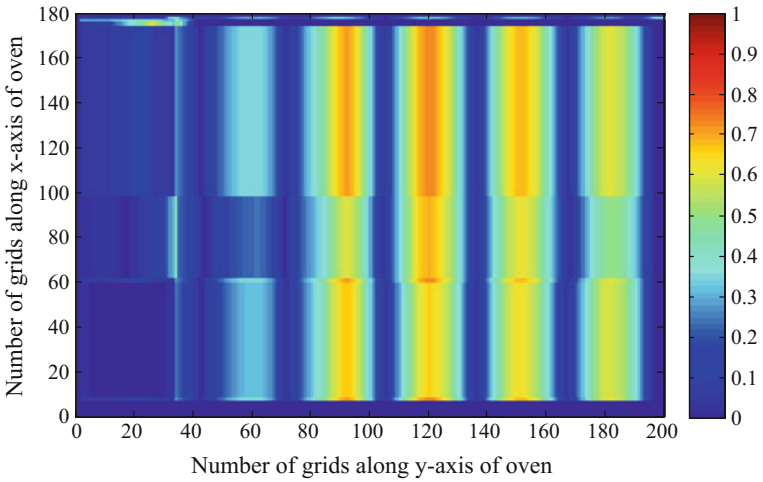

Fig. 6 Normalized total electric field (magnitude) distribution inside the oven cavity in *xy*-plane at z = 20 mm

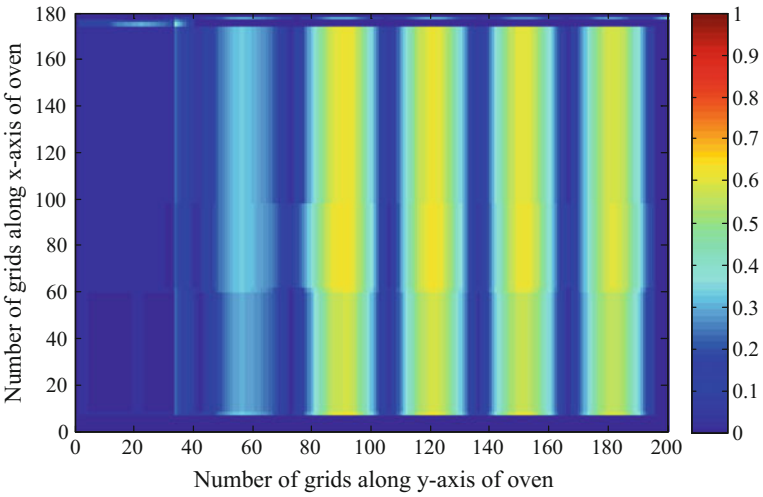

Fig. 7 Normalized total electric field (magnitude) distribution inside the oven cavity in *xy*-plane at z = 40 mm

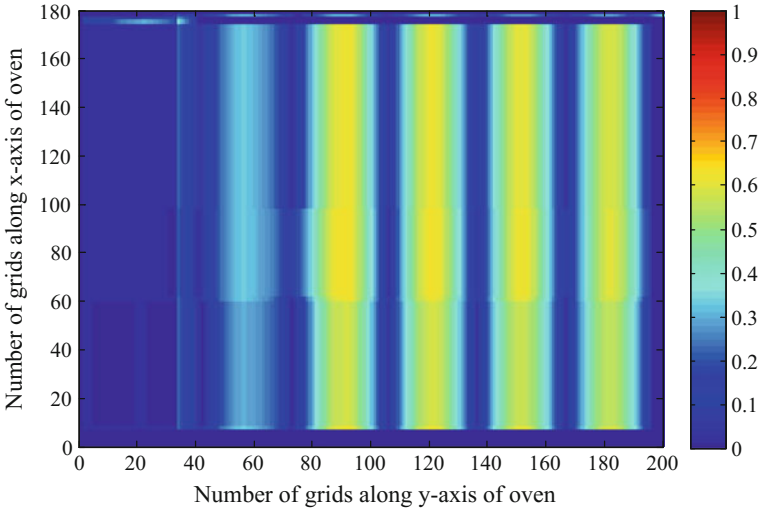

Fig. 8 Normalized total electric field (magnitude) distribution inside the oven cavity in *xy*-plane at z = 60 mm

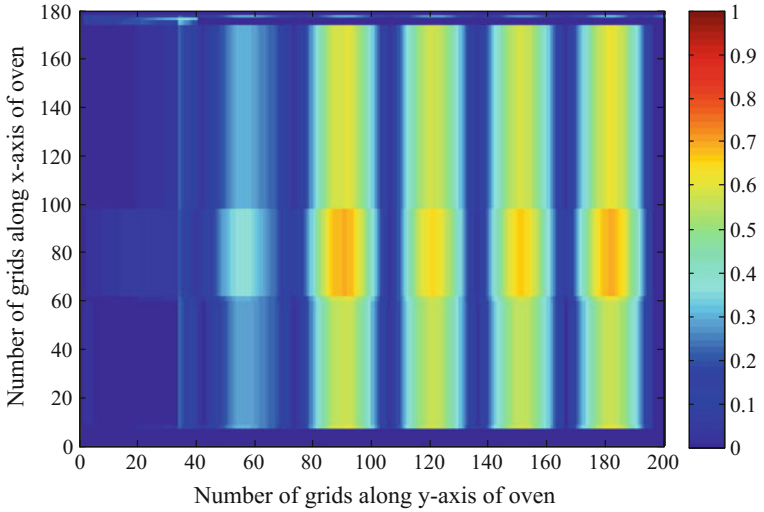

Fig. 9 Normalized total electric field (magnitude) distribution inside the oven cavity in *xy*-plane at z = 80 mm

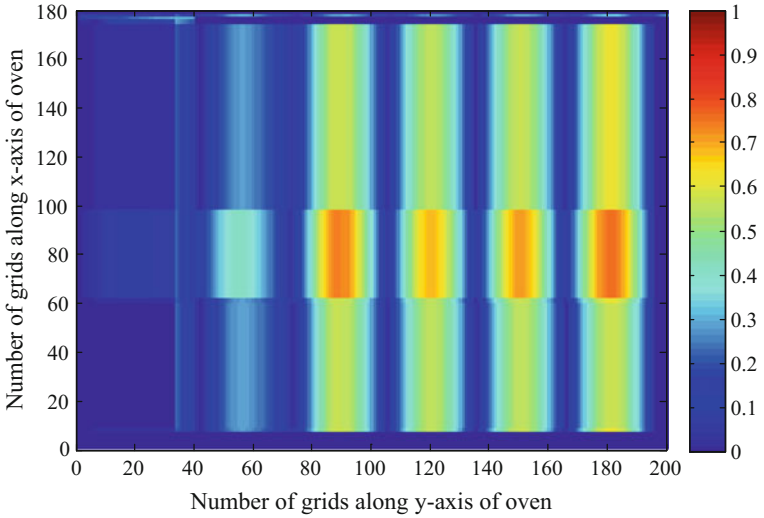

Fig. 10 Normalized total electric field (magnitude) distribution inside the oven cavity in *xy*-plane at z = 100 mm

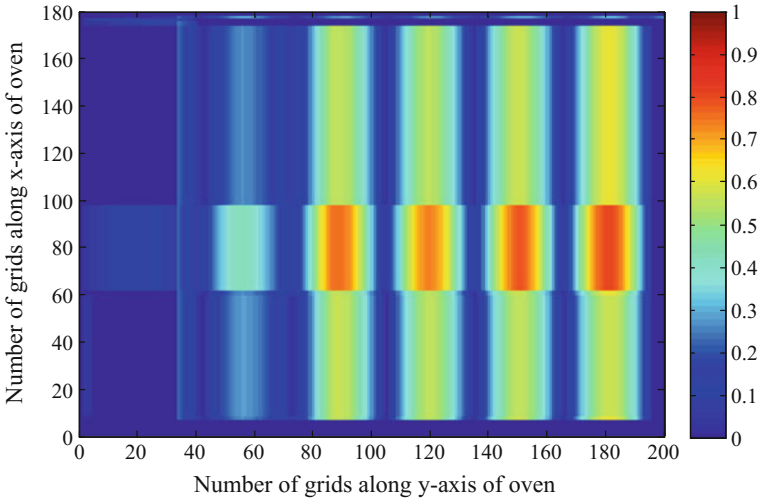

Fig. 11 Normalized total electric field (magnitude) distribution inside the oven cavity in *xy*-plane at z = 120 mm

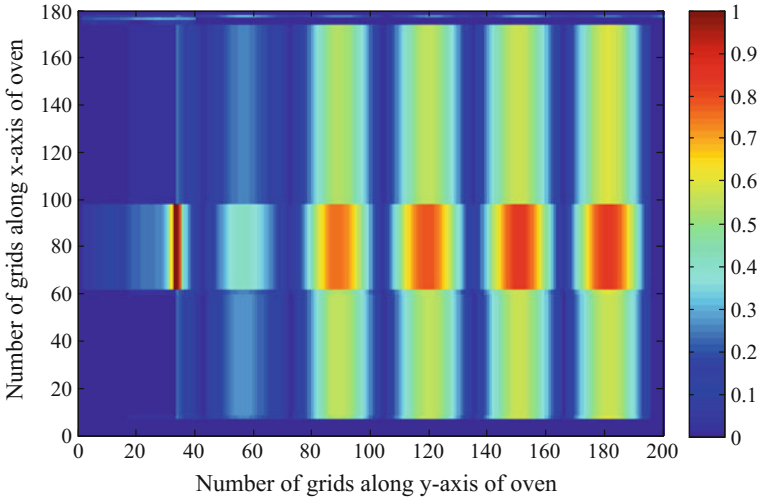

Fig. 12 Normalized total electric field (magnitude) distribution inside the oven cavity in *xy*-plane at z = 140 mm

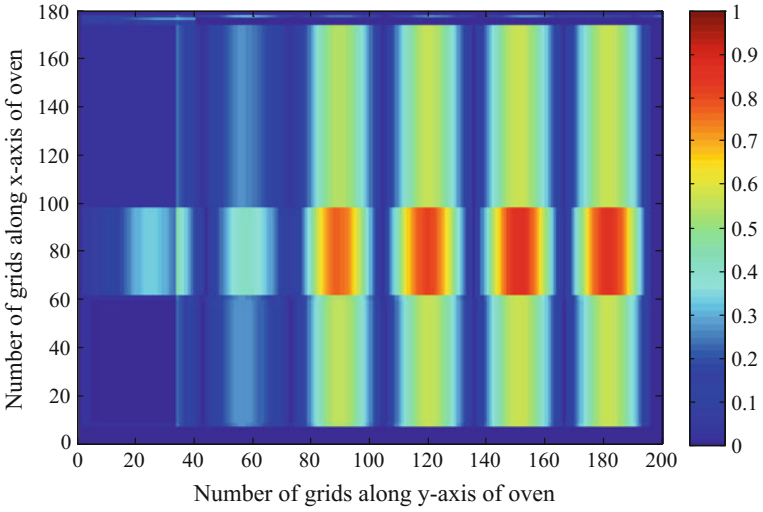

Fig. 13 Normalized total electric field (magnitude) distribution inside the oven cavity in *xy*-plane at z = 160 mm

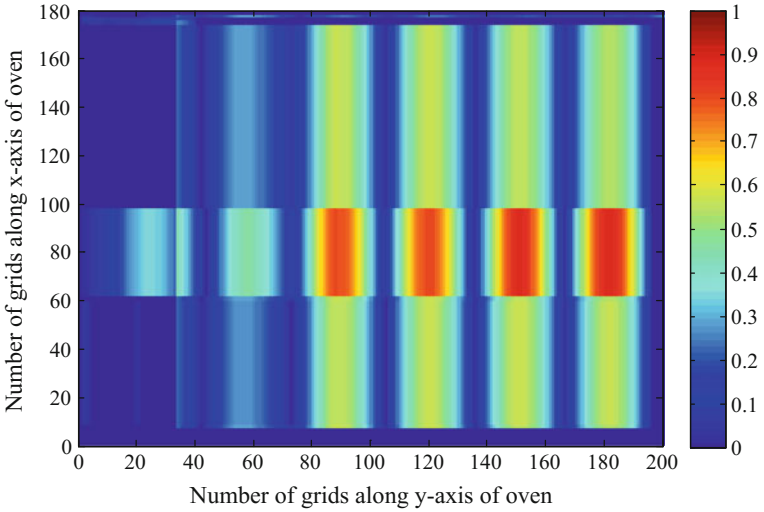

Fig. 14 Normalized total electric field (magnitude) distribution inside the oven cavity in *xy*-plane at z = 180 mm

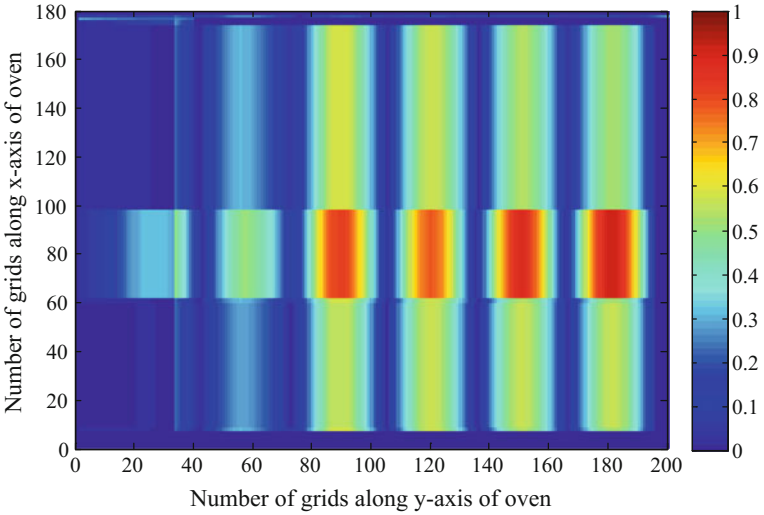

Fig. 15 Normalized total electric field (magnitude) distribution inside the oven cavity in *xy*-plane at z = 200 mm

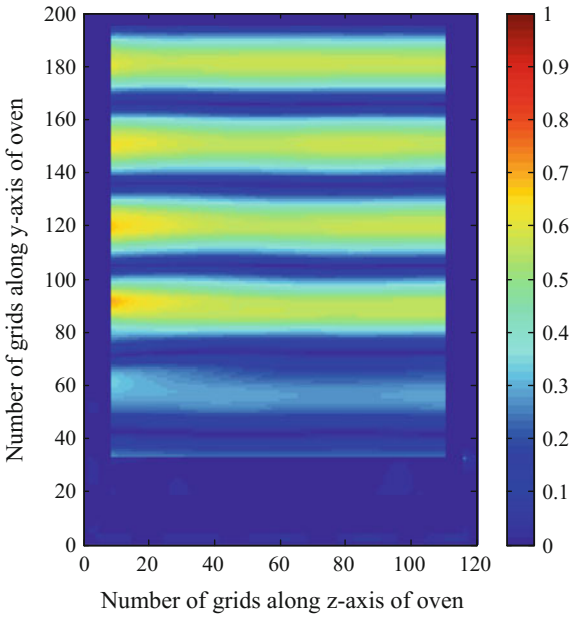

Fig. 16 Normalized total electric field (magnitude) distribution inside the oven in *yz*-plane at $x = 20$ mm

electric field distribution inside the cavity in *xy*-plane at different cuts along *z*-axis measured from bottom to top of the cavity (i.e., 20, 40, 60, 80, 100, 120, 140, 160, 180, and 200 mm). It is observed that the electric field is more uniform near to the bottom of the cavity as compared to the top side of the cavity in *xy*-plane. Here, a band in the middle portion of each of the Figs. 6, 7, 8, 9, 10, 11, 12, 13, 14, and 15 is observed to appear that is due to the presence of opening of the waveguide of magnetron source. Further, the total electric field (magnitude) distribution inside the cavity is studied in *yz*-plane at different cuts along *x*-axis measured from back to front of the cavity as shown in Figs. 16, 17, 18, 19, 20, 21, 22, 23, 24, and 25. Finally, the total electric field distribution inside the oven cavity is determined in *zx*-plane at different cuts along y-axis measured from right to left of cavity as shown in Figs. 26, 27, 28, 29, 30, 31, 32, 33, 34, and 35. Here, a band appears in the middle portion of *zx*-plane at all cuts due to the effect of magnetron source wave guide.

To conclude, the total electric field distribution inside the oven is not uniform in all planes. Moreover, it varies with respect to different cuts in each plane. The amplitude of field distribution in *xy*- and *yz*-planes of the oven cavity is better than that of *zx*-plane. In order to have uniform field distribution inside the oven cavity, the position of microwave source needs to be optimized.

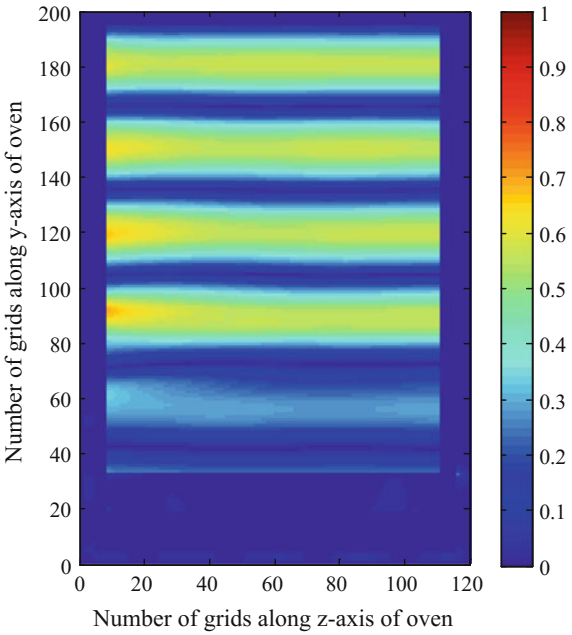

Fig. 17 Normalized total electric field (magnitude) distribution inside the oven in *yz*-plane at x = 60 mm

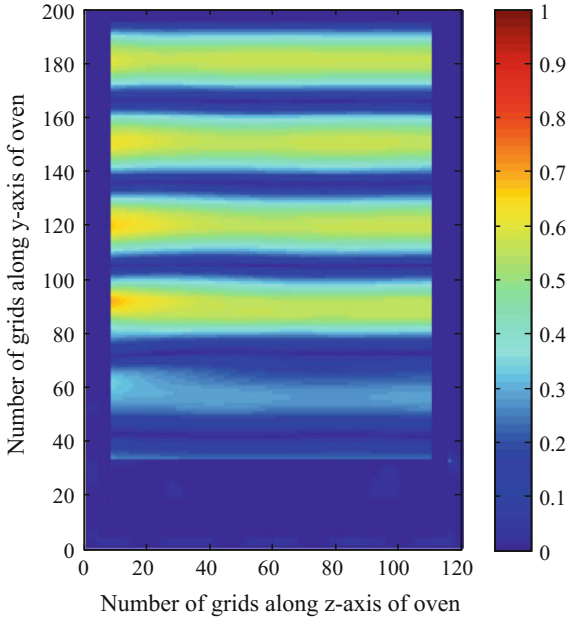

Fig. 18 Normalized total electric field (magnitude) distribution inside the oven in *yz*-plane at x = 100 mm

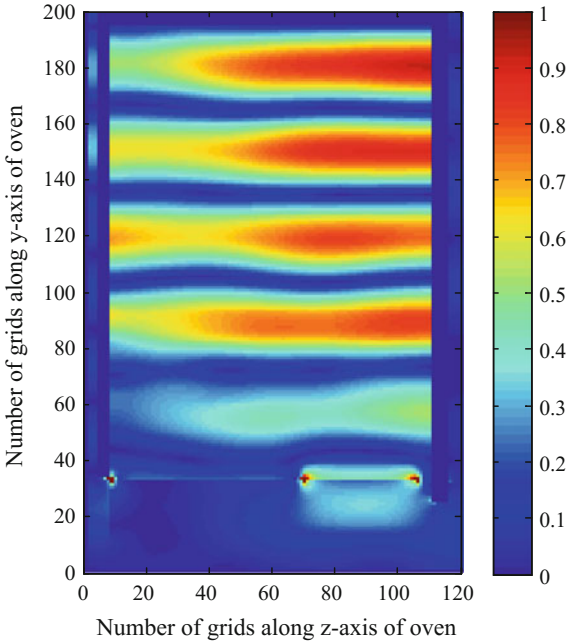

Fig. 19 Normalized total electric field (magnitude) distribution inside the oven in *yz*-plane at x = 140 mm

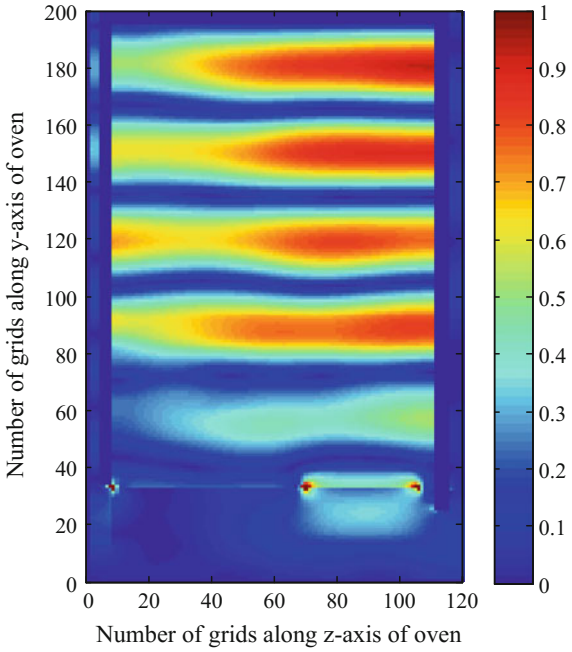

Fig. 20 Normalized total electric field (magnitude) distribution inside the oven in *yz*-plane at x = 180 mm

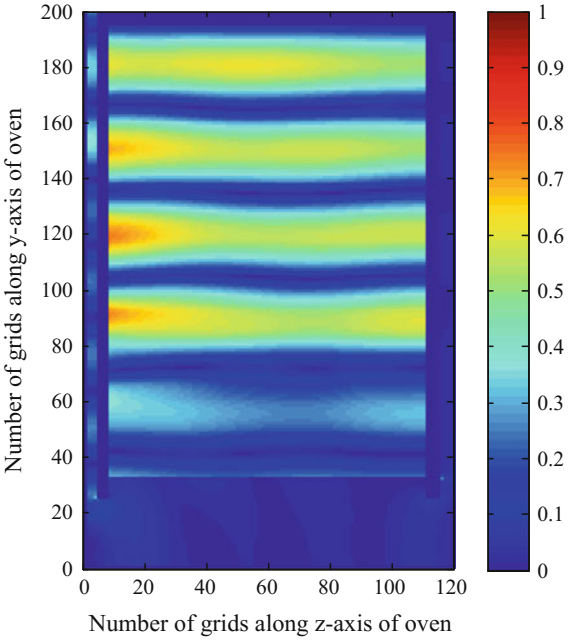

Fig. 21 Normalized total electric field (magnitude) distribution inside the oven in *yz*-plane at x = 220 mm

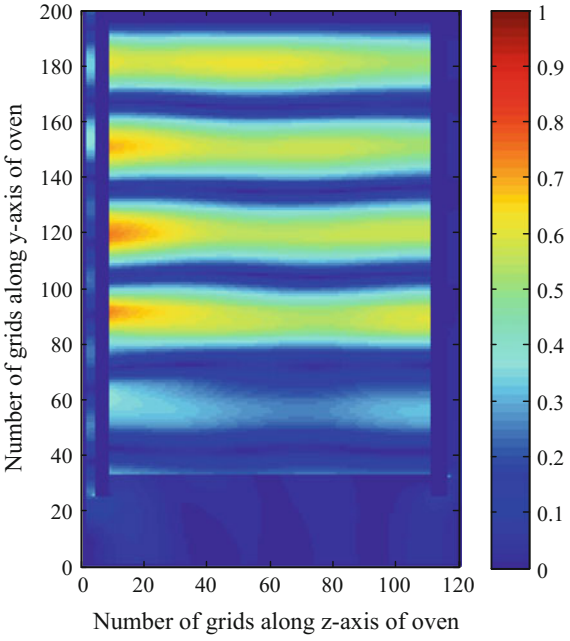

Fig. 22 Normalized total electric field (magnitude) distribution inside the oven in *yz*-plane at x = 260 mm

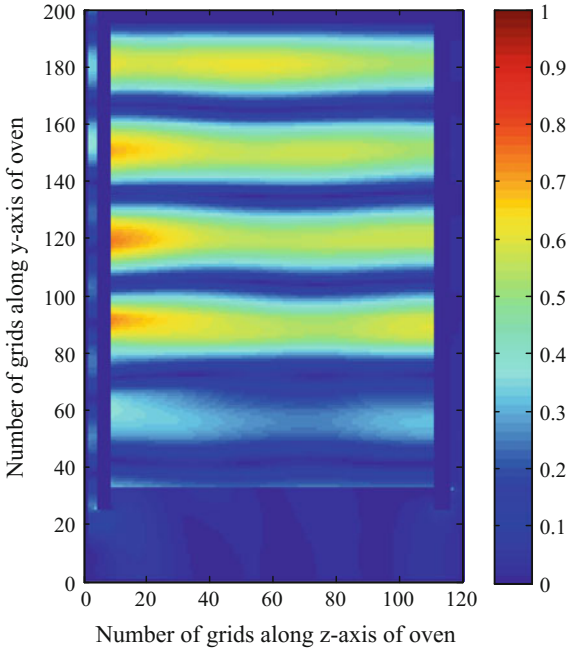

Fig. 23 Normalized total electric field (magnitude) distribution inside the oven in *yz*-plane at x = 300 mm

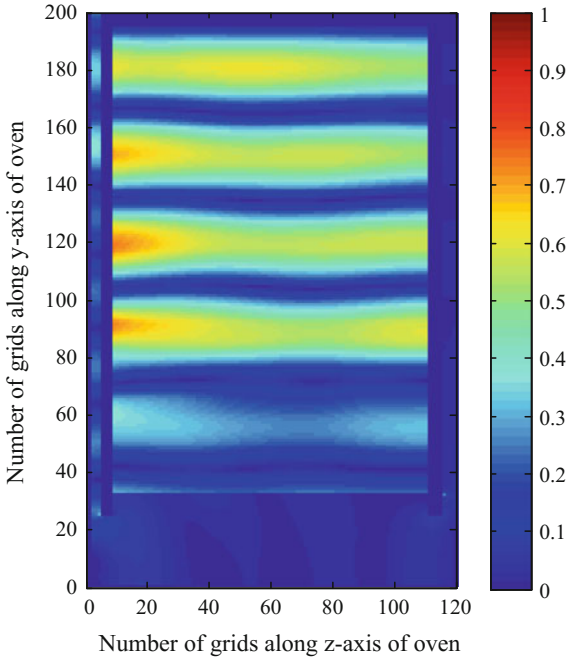

Fig. 24 Normalized total electric field (magnitude) distribution inside the oven in *yz*-plane at x = 320 mm

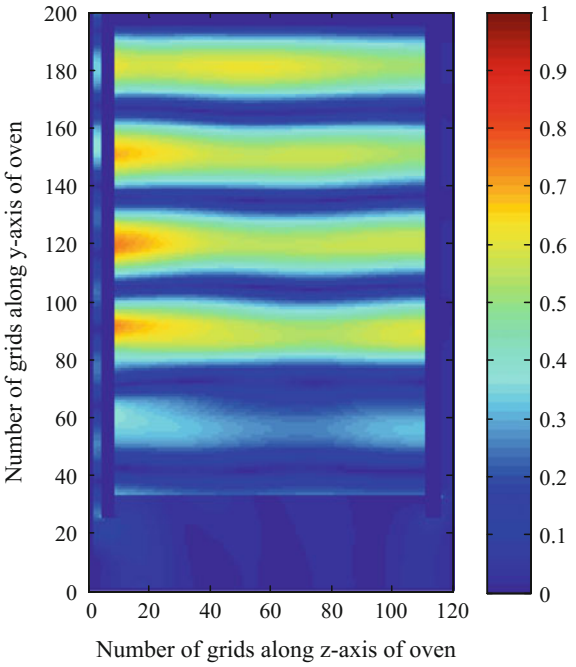

Fig. 25 Normalized total electric field (magnitude) distribution inside the oven in *yz*-plane at x = 340 mm

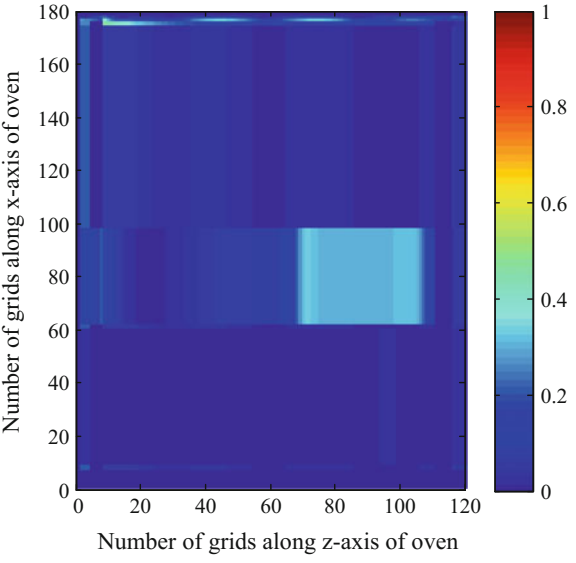

Fig. 26 Normalized total electric field (magnitude) distribution inside the oven in *zx*-plane at y = 60 mm

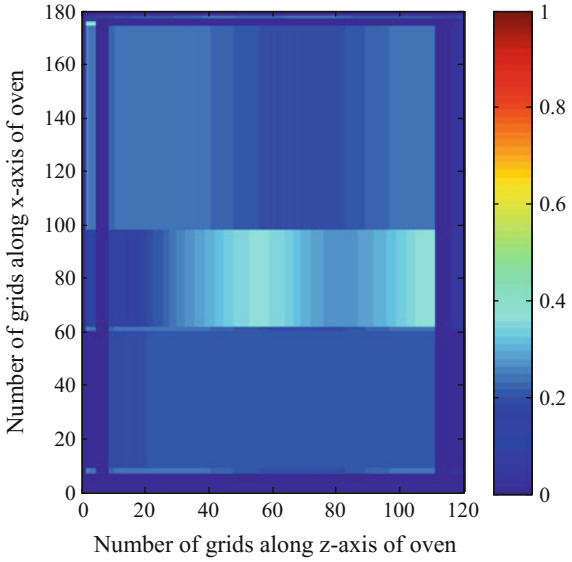

Fig. 27 Normalized total electric field (magnitude) distribution inside the oven in *zx*-plane at y = 100 mm

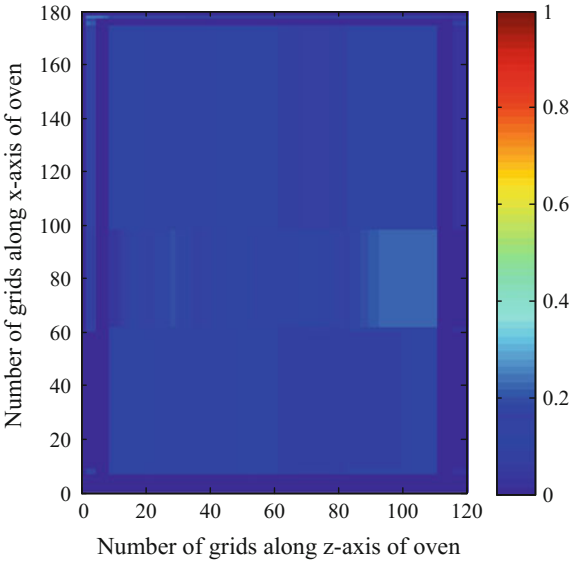

Fig. 28 Normalized total electric field (magnitude) distribution inside the oven in *zx*-plane at y = 140 mm

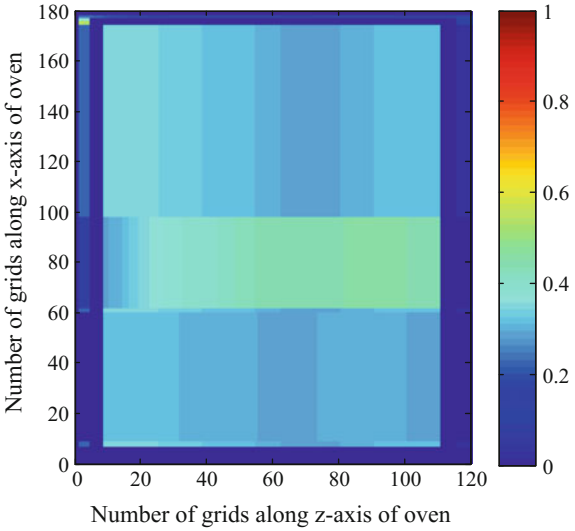

Fig. 29 Normalized total electric field (magnitude) distribution inside the oven in *zx*-plane at y = 160 mm

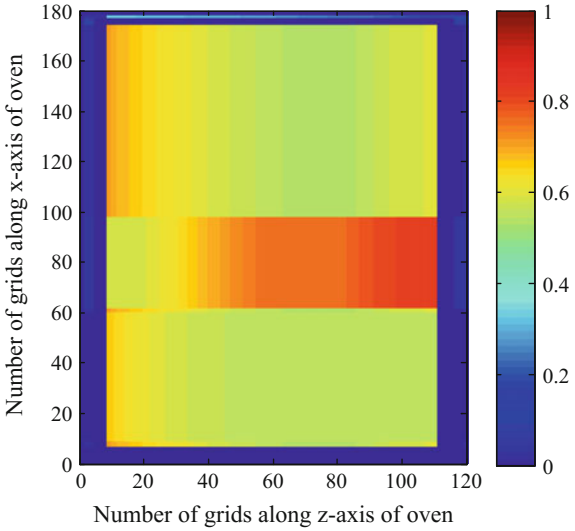

Fig. 30 Normalized total electric field (magnitude) distribution inside the oven in *zx*-plane at y = 180 mm

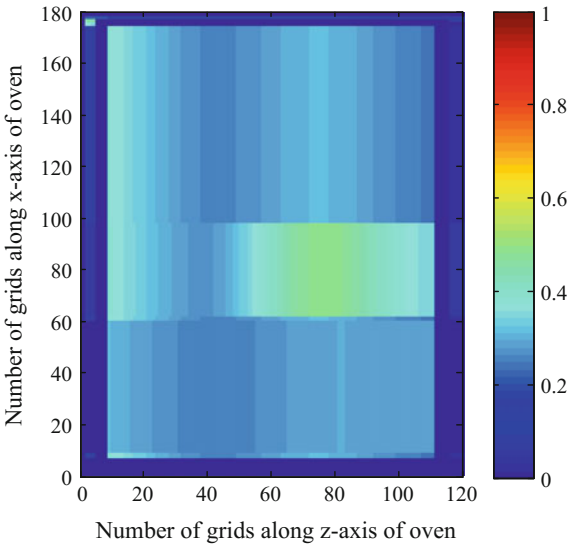

Fig. 31 Normalized total electric field (magnitude) distribution inside the oven in *zx*-plane at y = 220 mm

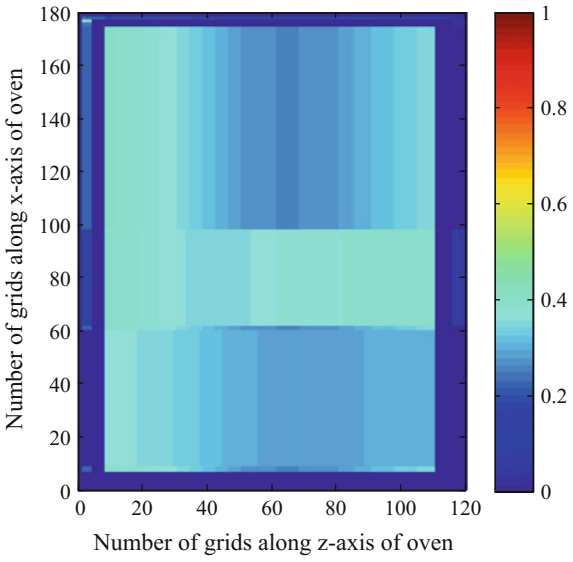

Fig. 32 Normalized total electric field (magnitude) distribution inside the oven in *zx*-plane at y = 260 mm

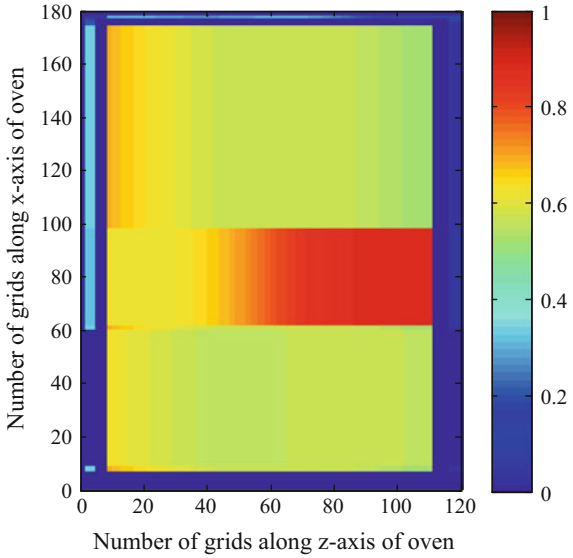

Fig. 33 Normalized total electric field (magnitude) distribution inside the oven in *zx*-plane at y = 300 mm

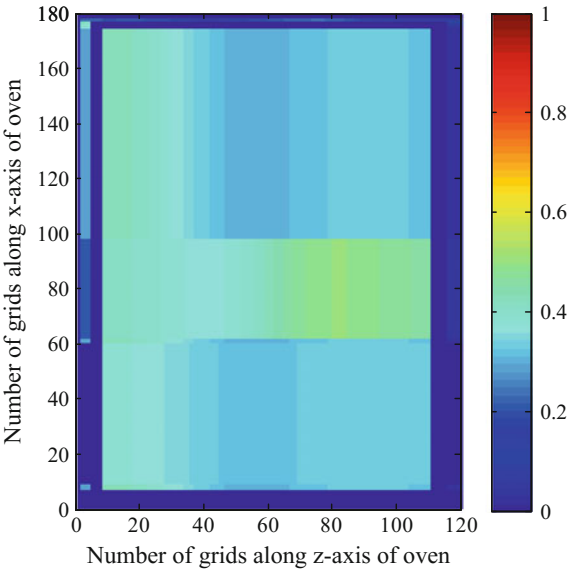

Fig. 34 Normalized total electric field (magnitude) distribution inside the oven in *zx*-plane at y = 320 mm

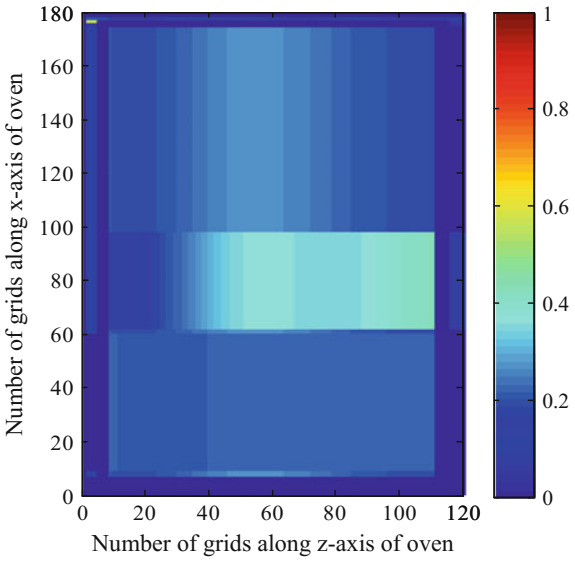

Fig. 35 Normalized total electric field (magnitude) distribution inside the oven in *zx*-plane at y = 340 mm

4 Modeling of Curved Cavities Using FDTD

A uniform grid is very efficient for computing the inner domain of homogeneous medium. However, modeling curved interfaces and boundaries, the approximation becomes coarse because it is difficult to properly resolve the geometry using only horizontal and vertical planes. This gives rise to *Lego effect*, where objects modeled obtain a distinct block-shaped look. In order to model curved surface in FDTD, the method used here is a stepped surface approximation called *staircasing*. The staircase approximation is a method to represent a smooth transition between two media (Taflove and Hagness 2005). In this approximation, each FDTD cell is split up into subcells and the average dielectric properties are determined according to the number of subcells in the first medium and in the other one. In staircase approach, a continuous chain of zeros in the E_x and E_y values will represent a perfect electric conductor boundary. The subcells give freedom to represent this chain of zeros for curved structures along their diagonals. So the probability of error in the staircase approximation-based modeling is reduced compared to the uniform grid approximation.

In order to deal with a conformal structure, initially the overall problem space is assumed to be free space. So, each cell is initialized to the values of permittivity, ε, and conductivity, σ. Then each cell is divided into n number of subcells along x- and y-axes. If the distance from the center to each subcell is within the radius, the contribution of dielectric properties is added to the total $\varepsilon[n]$ and $\sigma[n]$ by subtracting the previous values of $\varepsilon[n-1]$ and $\sigma[n-1]$ as given below (Sullivan 2000):

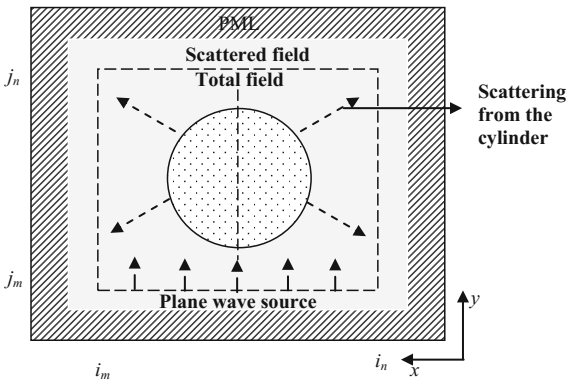

Fig. 36 FDTD modeling of 2D dielectric cylinder illuminated by plane wave

$$\text{eps} = \text{eps} + \left(\frac{1}{n^2}\right)(\varepsilon[n] - \varepsilon[n-1]) \tag{18}$$

$$\text{cond} = \text{cond} + \left(\frac{1}{n^2}\right)(\sigma[n] - \sigma[n-1]) \tag{19}$$

4.1 Validation of FDTD Modeling for Curved Structure

In order to examine the efficacy of the staircase approach, EM analysis of scattered field from a dielectric cylinder illuminated by a plane wave is carried out using 2D FDTD method. The FDTD simulation of the plane wave striking on a dielectric cylinder is shown in Fig. 36. To simulate such geometry illuminated with plane wave source, the problem space is divided into *total field* and *scattered field* region. This is performed to avoid the interaction of propagating wave with the absorbing boundary and to minimize the reflection load on the absorbing boundary conditions. The error arising due to imperfect boundary can be reduced by subtracting the incident field and hence reducing the number of waves hitting the boundary (Taflove and Browdwin 1975).

In a two-dimensional FDTD model, entire field (electric or magnetic) will be either in the scattered field region or in the total field region. If a point locates within the total field, it uses the field values from outside to calculate the spatial derivatives. On the other hand, if a point is positioned within the scattered field region, it uses the values from the total field region. Such discrepancies need to be modified, which can be accomplished by correcting the fields at three boundaries as follows:

1. The electric field density, D_z values at $j = j_m$ or $j = j_n$

$$D_z(i,j_m) = D_z(i,j_m) + 0.5 \cdot H_{x\_inc}(j_m - 1/2) \tag{20a}$$

$$D_z(i,j_n) = D_z(i,j_n) - 0.5 \cdot H_{x\_inc}(j_n + 1/2) \tag{20b}$$

2. The magnetic field, H_x just outside $j = j_m$ and $j = j_n$

$$H_x(i,j_m - 1/2) = H_x(i,j_m - 1/2) + 0.5 \cdot E_{z\_inc}(j_m) \tag{21a}$$

$$H_x(i,j_n + 1/2) = H_x(i,j_n + 1/2) - 0.5 \cdot E_{z\_inc}(j_n) \tag{21b}$$

3. The H_y field just outside $i = i_m$ and $i = i_n$

$$H_y(i_m - 1/2,j) = H_x(i_m - 1/2,j) - 0.5 \cdot E_{z\_inc}(j) \tag{22a}$$

$$H_y(i_n + 1/2,j) = H_y(i_n + 1/2,j) + 0.5 \cdot E_{z\_inc}(j) \tag{22b}$$

where H_{x_inc} and E_{z_inc} represent the magnetic and electric field components of the incident plane wave. To assess the efficacy of the code, the computed scattered field from the dielectric cylinder is validated with the reported results (Sullivan, 2000) for the design parameters: diameter of the cylinder, 20 cm; dielectric permittivity, $\varepsilon_r = 30$; and conductivity, $\sigma = 0.3$. In the FDTD simulation, the problem space is first assumed to be free space and each cell is divided into nine subcells. The distance of each cell from the center of the problem space is then calculated. The size of cell is considered to be 10 mm at frequency 0.3 GHz. Finally, the cylinder is modeled using the below conditions:

If distance $\leq$ cylinder radius
$\varepsilon = 30$ and $\sigma = 0.3$
Else $\varepsilon = 1$ and $\sigma = 0$.

The contribution of the dielectric properties to the total effective permittivity and conductivity is determined from Eqs. (18) and (19). The scattered field from dielectric cylinder is computed for the time steps, 25, 50, and 75, as shown in Figs. 37, 38, and 39, respectively, and is validated with the reported results given in Sullivan (2000). Excellent agreement is observed between computed and reported results.

4.2 *EM Analysis of Field Distribution Inside the Hybrid-Cylindrical Microwave Autoclave*

The EM analysis of field distribution inside the cylindrical microwave autoclave is carried out in this work using three-dimensional FDTD method. The schematic of

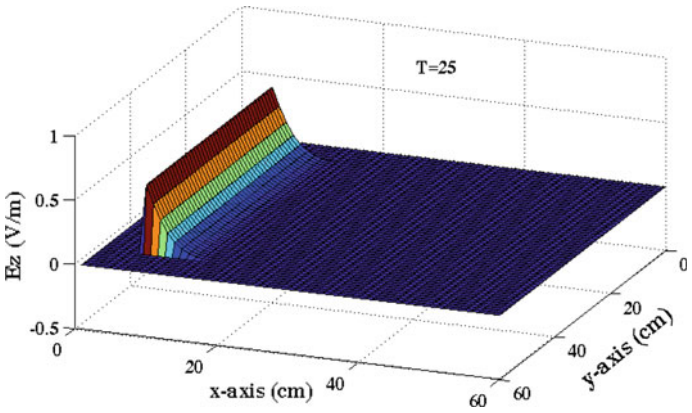

Fig. 37 E_z component of plane wave impinging on a dielectric cylinder at time step, $T = 25$

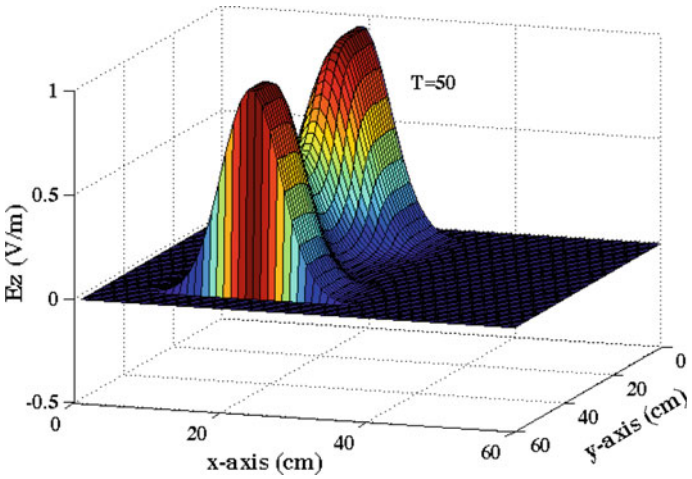

Fig. 38 E_z component of plane wave impinging on a dielectric cylinder at time step, $T = 50$

hybrid-cylindrical microwave autoclave is shown in Fig. 40, which mainly consists of a cylindrical cavity. The cavity is excited with TE_{11} mode of plane wave by multiple magnetron sources, viz, S_1, S_2, S_3, S_4, and S_5 through circular waveguide feed. This plane wave propagates inside the cavity and reflects back and forth from the cavity walls, resulting in the formation of standing waves inside the cavity. The autoclave here works on the principle of microwave heating. The dimension of the proposed cylindrical autoclave is given in Table 1.

A circular turntable is employed to generate a time-averaged uniform microwave field to achieve uniform heating within the cavity. The turntable is mounted over the metallic plate, which is extended along the length of the cylinder. The region

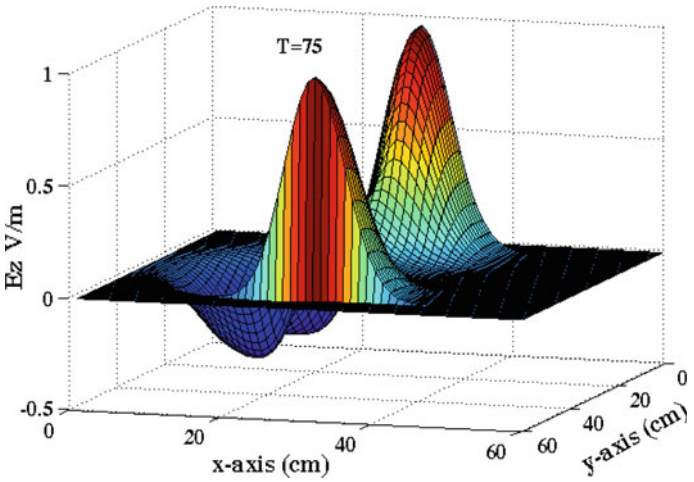

Fig. 39 E_z component of plane wave impinging on a dielectric cylinder at time step, $T = 75$

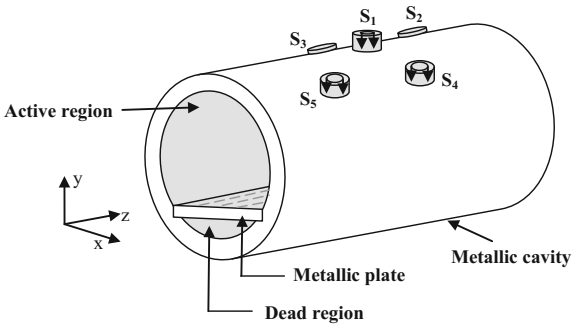

Fig. 40 Schematic of hybrid-cylindrical microwave autoclave

above the plate is the area of interest, where EM field distribution is intended to be determined. This is called as the *active region* of the autoclave. The region below the metal plate is a shadow region, where the propagation of EM field is completely blocked by the metal plate and is termed as *dead region*.

The representation of plane wave in three dimensions is similar to that of two dimensions except an additional surface (i.e., k surface). The consideration of EM fields in three dimensions is represented in Fig. 41. Here, a plane wave is assumed to be generated from a plane of the problem space. If it is considered to be in zx-plane, the plane wave will be added at $j = j_m$ and subtracted out at $j = j_n$. This is accomplished by adding to D or H fields which are on the boundary and subtracting out from those which are next to the boundary according to the expressions from Eqs. (20a) to (22b). In addition, k_m and k_n surfaces are also considered in 3D FDTD simulation, as given in Eq. (23a, 23b)

Table 1 Design dimensions of hybrid-cylindrical microwave autoclave

Design parameters	Dimension (mm)
Length of the cylinder	1500
Working diameter	790
Distance of the table from the top	620
Diameter of the source waveguide	100
Length of the source waveguide	40

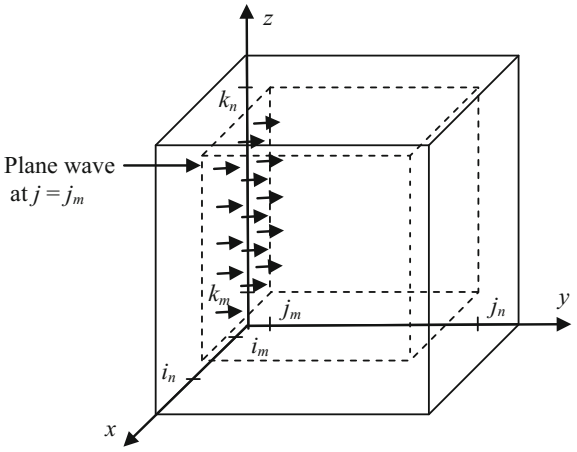

Fig. 41 Total and scattered field in 3D FDTD simulation

$$D_y(i, j+1/2, k_a) = D_y(i, j+1/2, k_a) - 0.5 \cdot H_{x\_inc}(j) \tag{23a}$$

$$D_y(i, j+1/2, k_b+1) = D_y(i, j+1/2, k_b+1) - 0.5 \cdot H_{x\_inc}(j) \tag{23b}$$

According to FDTD method, the whole space of EM analysis is divided into multiple small lattices, and electrical constants are assigned to each lattice. The cell size is taken to be $\Delta x = \Delta y = \Delta z = 5$ mm with respect to the operating frequency, 2.45 GHz. The perfect electric conductor (PEC) boundary is applied to the metal surfaces, and perfectly matched layer (PML) boundary is applied to the whole analysis structure as absorbing boundary. The EM field distributions inside the cylindrical autoclave are determined by exciting it with a single as well as five magnetron sources. The details of the EM analysis are discussed in the following subsections.

4.2.1 EM Field Distribution Due to Single Magnetron Source

The EM field distribution inside the microwave cylindrical autoclave is determined by exciting it with a single magnetron source S_1, leaving all other sources short. In FDTD simulation, the actual dimensions of the hybrid-cylindrical autoclave are

scaled down to 4, i.e., 1:4 ratios. In order to keep operating frequency fixed at 2.45 GHz, the magnetron source waveguide (cylindrical feed) has not been scaled down. The excitation function for exciting the autoclave through circular waveguide source S_1 is expressed by (Liao 1995)

$$E_r = \left[E_{0r} \cdot J_n\left(\frac{X'_{\mathrm{np}} \cdot r}{a}\right)\right] \cdot \mathrm{Sin}(n\phi)\, \mathrm{e}^{-j\beta_g y} \tag{24a}$$

where r represents the distance along radial direction of circular waveguide. β_g is the phase constant, a is the radius of circular source wave guide, X'_{np} is the zeros of Bessel function J_n, and E_{0r} is the magnitude of plane wave. The first subscript n represents the full cycle of wave along circumference of circular waveguide, and p is the number of zeros of ϕ-direction electric field along the radial direction of circular waveguide. For TE_{11} mode, the Eq. (24a) is represented as

$$E_r = \left[E_{0r} \cdot J_1\left(\frac{X_{11} r}{a}\right)\right] \cdot \mathrm{Sin}(n\phi)\, \mathrm{e}^{-j\beta_g y} \tag{24b}$$

The value of $J_1\left(\frac{X_{11} r}{a}\right)$ is 0.58 at $r = a$. Hence, the value of expression inside the square bracket will be a numerical value, which is taken to be 1 V/m in the FDTD analysis for simplicity.

The EM field distribution inside the hybrid-autoclave is studied in *xy*-, *yz*- and *zx*-planes of the autoclave for 600 time steps using 3D FDTD method as FDTD solution is getting converge at chosen time step. Figures 42, 43, 44, 45, and 46

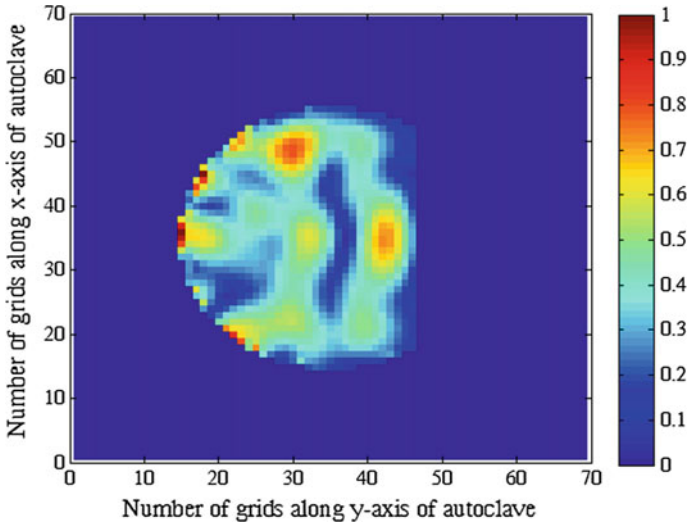

Fig. 42 Normalized total electric field (magnitude) distribution inside the hybrid-cylindrical autoclave in *xy*-plane at $z = 95$ mm

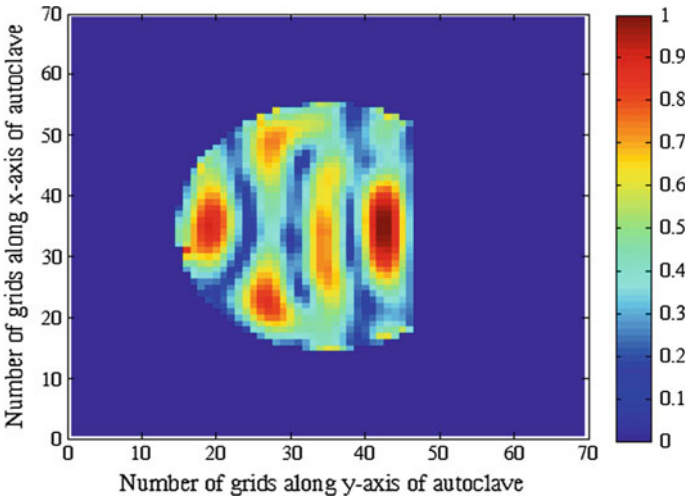

Fig. 43 Normalized total electric field (magnitude) distribution inside the hybrid-cylindrical autoclave in *xy*-plane at z = 175 mm

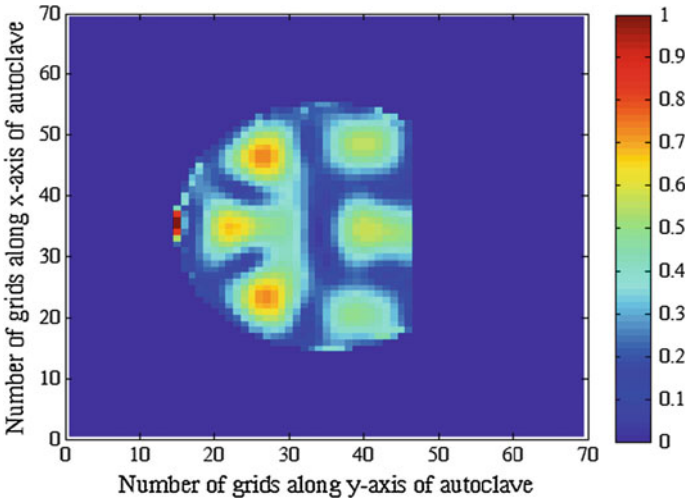

Fig. 44 Normalized total electric field (magnitude) distribution inside the hybrid-cylindrical autoclave in *xy*-plane at z = 235 mm

represent the electric field distribution inside the autoclave in *xy*-plane at different cuts along z-axis (i.e., at z = 95, 175, 235, 315, and 455 mm) measured from front to back side of the autoclave. It is observed that the field is fully distributed inside the autoclave cavity across the *xy*-cross section. However, amplitude of field distribution is not uniform corresponding to different cuts along z-axis.

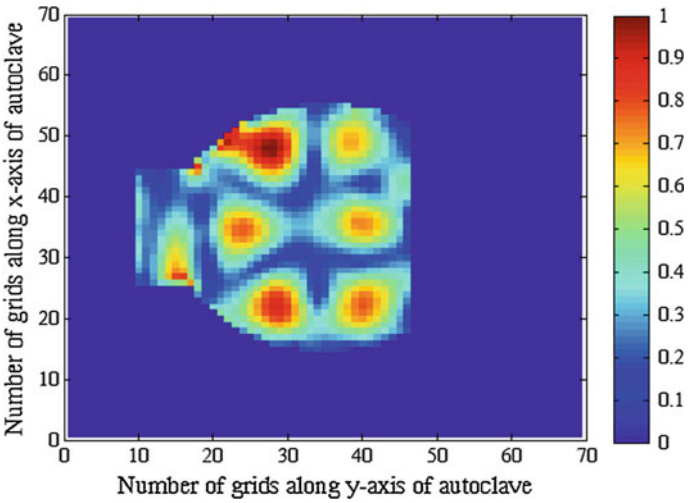

Fig. 45 Normalized total electric field (magnitude) distribution inside the hybrid-cylindrical autoclave in *xy*-plane at $z = 315$ mm

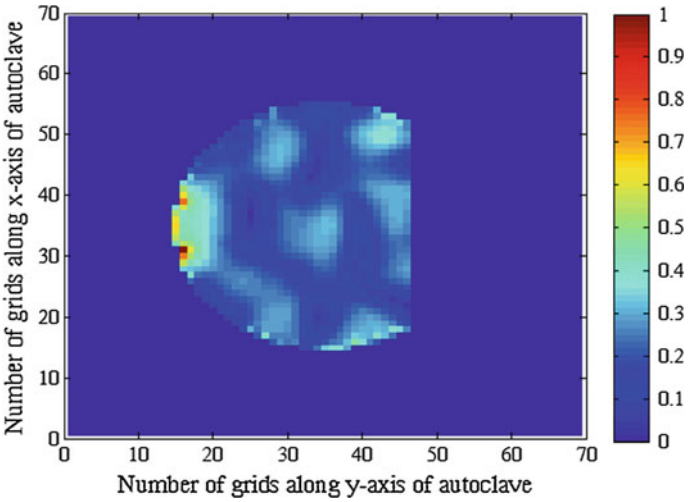

Fig. 46 Normalized total electric field (magnitude) distribution inside the hybrid-cylindrical autoclave in *xy*-plane at $z = 455$ mm

Further, the electric field distribution inside the cavity is studied in *yz*-plane at different cuts along *x*-axis (i.e., at $x = 85$, 145, 205, and 265 mm) measured from left side to right side of the autoclave as shown in Figs. 47, 48, 49, and 50. It is observed that the field distribution inside autoclave cavity is not uniform in *yz*-plane corresponding to all cuts along *x*-axis. However, as we move from either left or

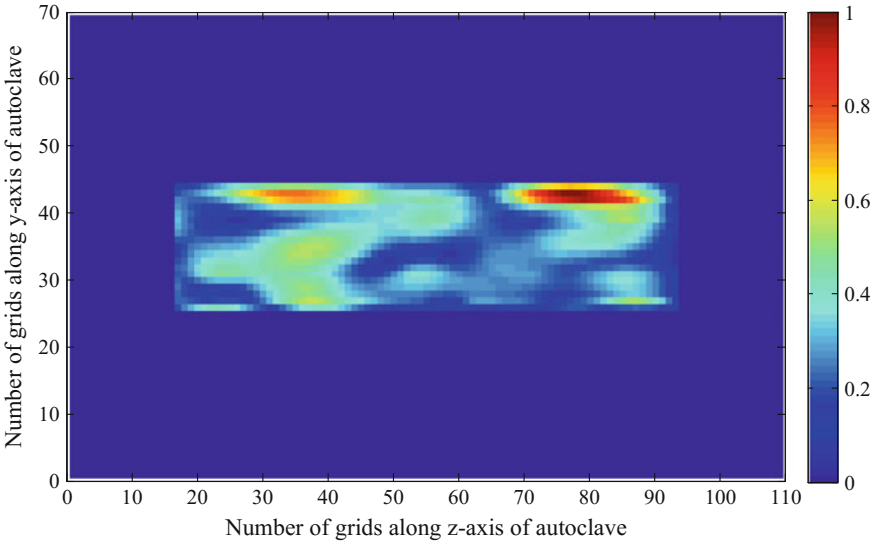

Fig. 47 Normalized total electric field (magnitude) distribution inside the hybrid-cylindrical autoclave in *yz*-plane at $x = 85$ mm

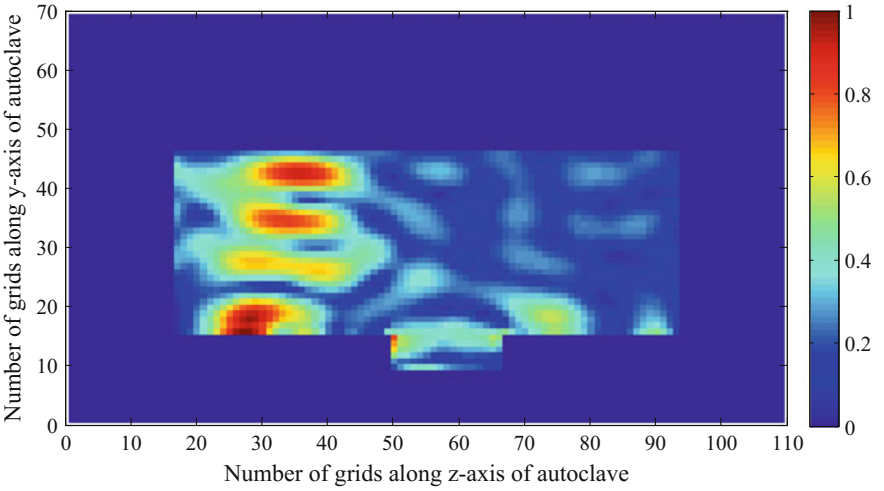

Fig. 48 Normalized total electric field (magnitude) distribution inside the hybrid-cylindrical autoclave in *yz*-plane at $x = 145$ mm

right toward the middle portion of the cavity along *x*-axis, the field distribution is observed to be more uniform. Finally, the electric field distribution inside the oven cavity is determined in *zx*-plane at different cuts along *y*-axis (i.e., at $y = 85$, 125, 155, 185, and 225 mm) measured from top to the bottom of the autoclave as shown

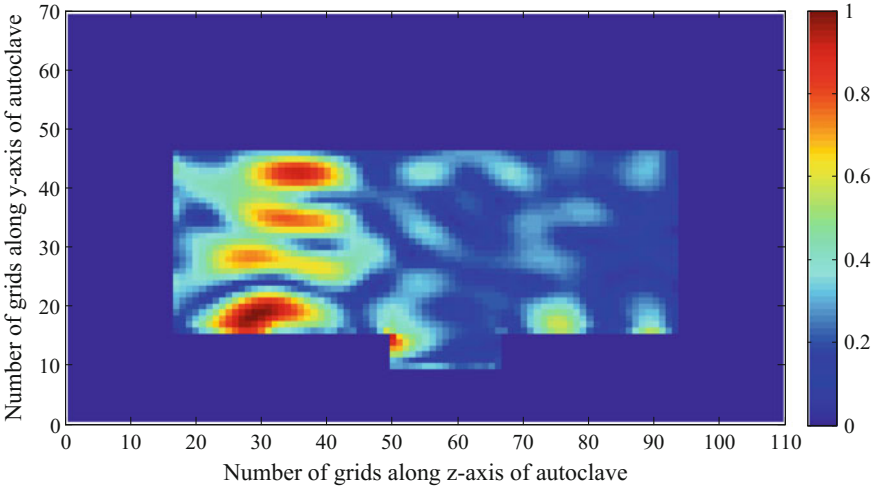

Fig. 49 Normalized total electric field (magnitude) distribution inside the cylindrical autoclave in *yz*-plane at $x = 205$ mm

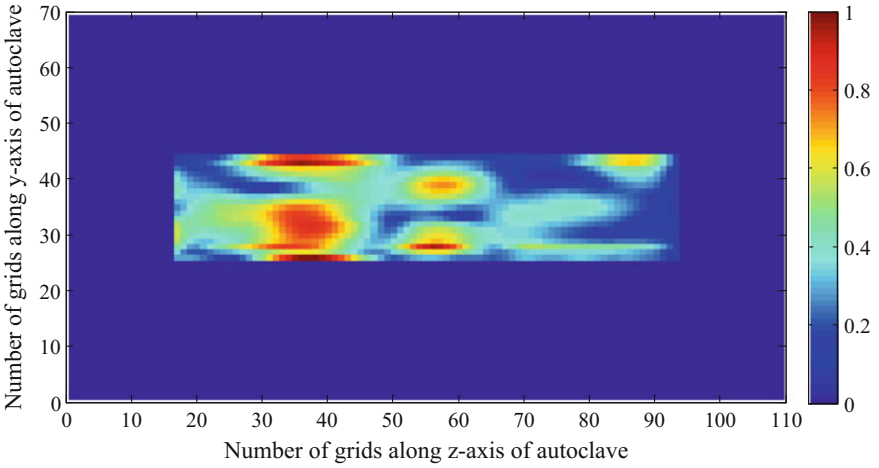

Fig. 50 Normalized total electric field (magnitude) distribution inside the hybrid-cylindrical autoclave in *yz*-plane at $x = 265$ mm

in Figs. 51, 52, 53, 54, and 55. It is observed that the field is not uniform in *zx*-plane except at $y = 155$ mm and $y = 225$ mm. Thus, it is concluded that the single magnetron source is not sufficient to achieve uniform field distribution inside the proposed autoclave cavity.

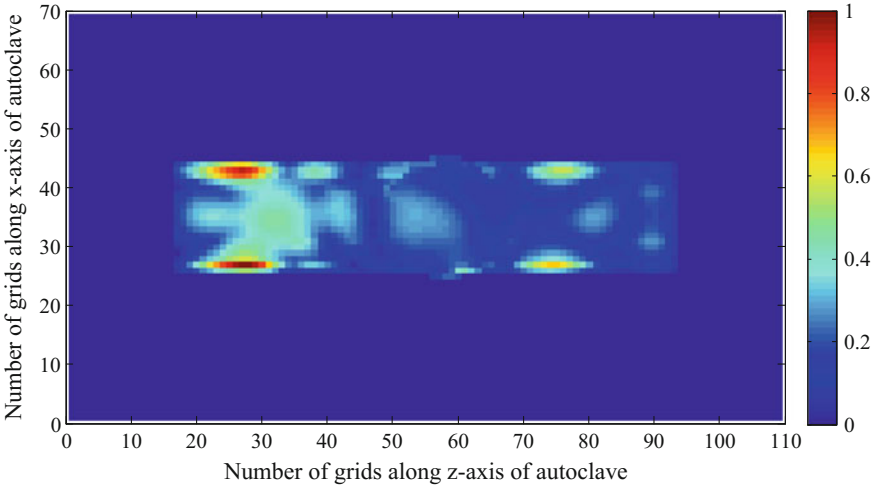

Fig. 51 Normalized total electric field (magnitude) distribution inside the hybrid-cylindrical autoclave in *zx*-plane at $y = 85$ mm

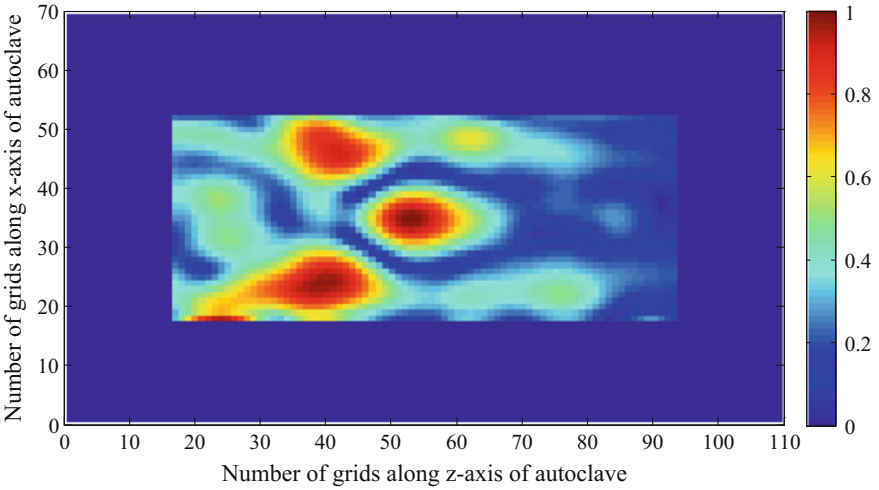

Fig. 52 Normalized total electric field (magnitude) distribution inside the hybrid-cylindrical autoclave in *zx*-plane at $y = 125$ mm

4.2.2 EM Field Distribution Due to Five Magnetron Sources

The EM field distribution inside the microwave hybrid-cylindrical autoclave is studied by exciting it with all five magnetron sources, viz, S_1, S_2, S_3, S_4, and S_5 through the circular waveguide aperture (Fig. 40). In this case, the design

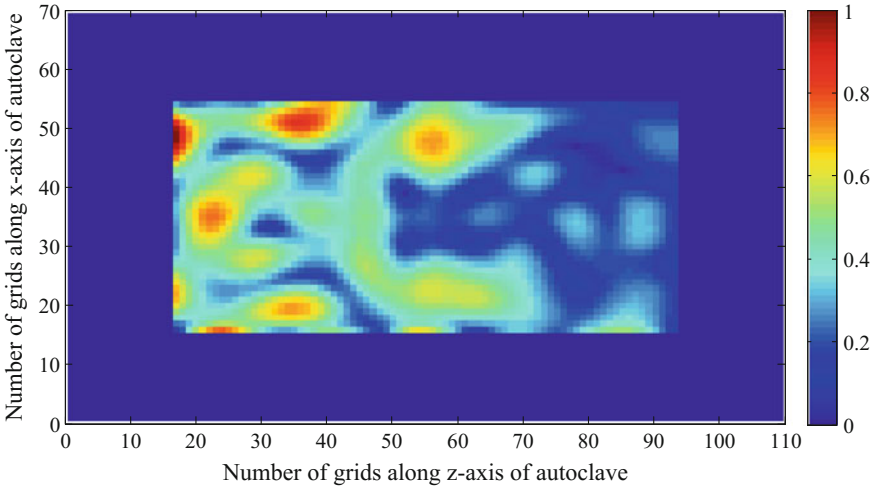

Fig. 53 Normalized total electric field (magnitude) distribution inside the hybrid-cylindrical autoclave in *zx*-plane at y = 155 mm

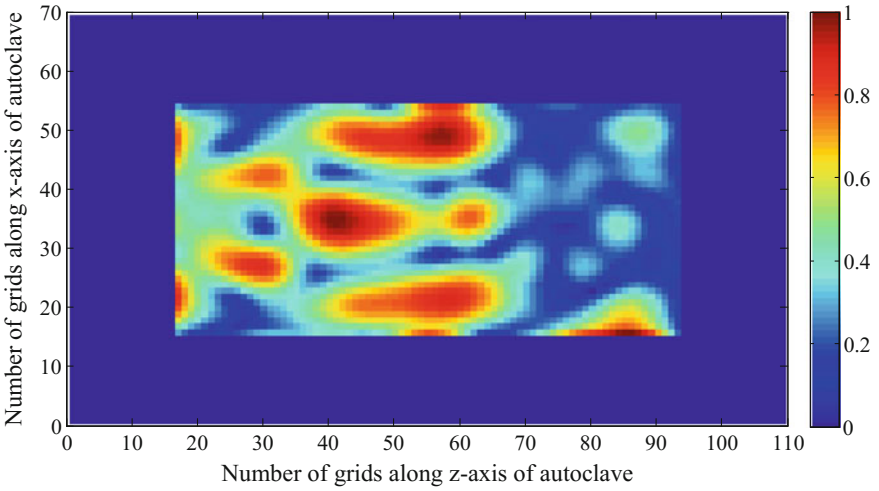

Fig. 54 Normalized total electric field (magnitude) distribution inside the hybrid-cylindrical autoclave in *zx*-plane at y = 185 mm

dimensions of the hybrid-cylindrical autoclave are scaled down to 1:2 ratios for FDTD analysis. In FDTD simulation, the locations of five magnetron sources are modeled with regard to scaled autoclave geometry as shown in Fig. 56a and compared with the actual locations of the sources (Fig. 56b). It is observed that the

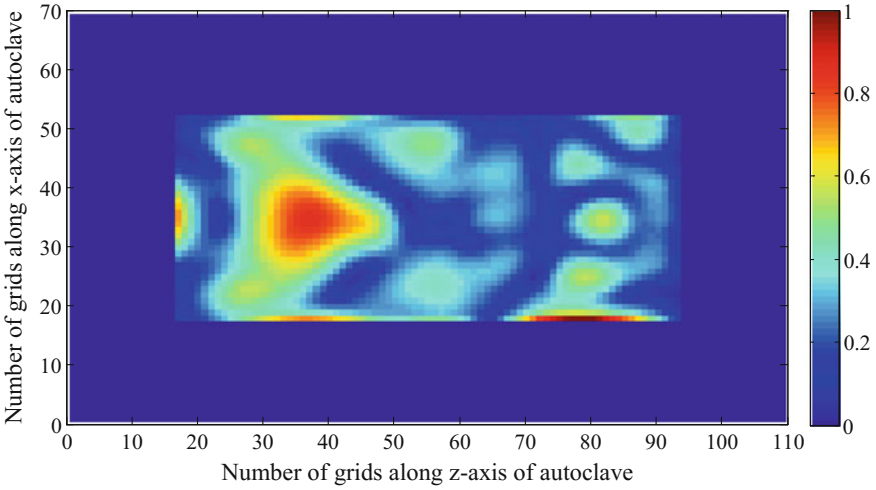

Fig. 55 Normalized total electric field (magnitude) distribution inside the hybrid-cylindrical autoclave in *zx*-plane at $y = 225$ mm

locations of five magnetron sources in FDTD modeling are exactly matching with their actual positions.

The dimensions of whole problem space in terms of grid number are considered to be 140, 140, and 220 along *x*-, *y*-, and *z*-axes, respectively (Fig. 41). The location of scaled down (1:2 ratio) hybrid-cylindrical autoclave cavity within the whole problem space is defined as

Along *x*-axis From $i = 30$th grid to $i = 110$th grid
Along *y*-axis From $j = 30$th grid to $j = 90$th grid
Along *z*-axis From $k = 34$th grid to $k = 184$th grid.

In order to examine the efficacy of the staircase approach, the EM field distribution inside scaled down (1:2 ratio) model of proposed autoclave cavity excited with single source (i.e., source, *S*1) is determined based on 3D FDTD in *xy*- and zx-planes at particular cut along z- and y-axes, respectively. The results obtained from the proposed FDTD (Figs. 57a and 58a) are compared with the corresponding results (Figs. 57b and 58b) obtained from the standard commercial EM software package. It is observed that the computed results obtained by the proposed FDTD method match well with the results obtained from the commercial software package.

Further, the electric field distribution inside the hybrid microwave autoclave is studied in *xy*-, *yz*-, and *zx*-planes of autoclave for 740 time steps using 3D FDTD method. Figures 59, 60, 61, 62, 63, 64, and 65 represent the electric field distribution inside the autoclave cavity in *xy*-plane at different cuts along *z*-axis (i.e., at $z = 190$, 290, 390, 590, 690, 890, and 910 mm) measured from front to back side of the autoclave. It is observed that the field is fully distributed across the circular

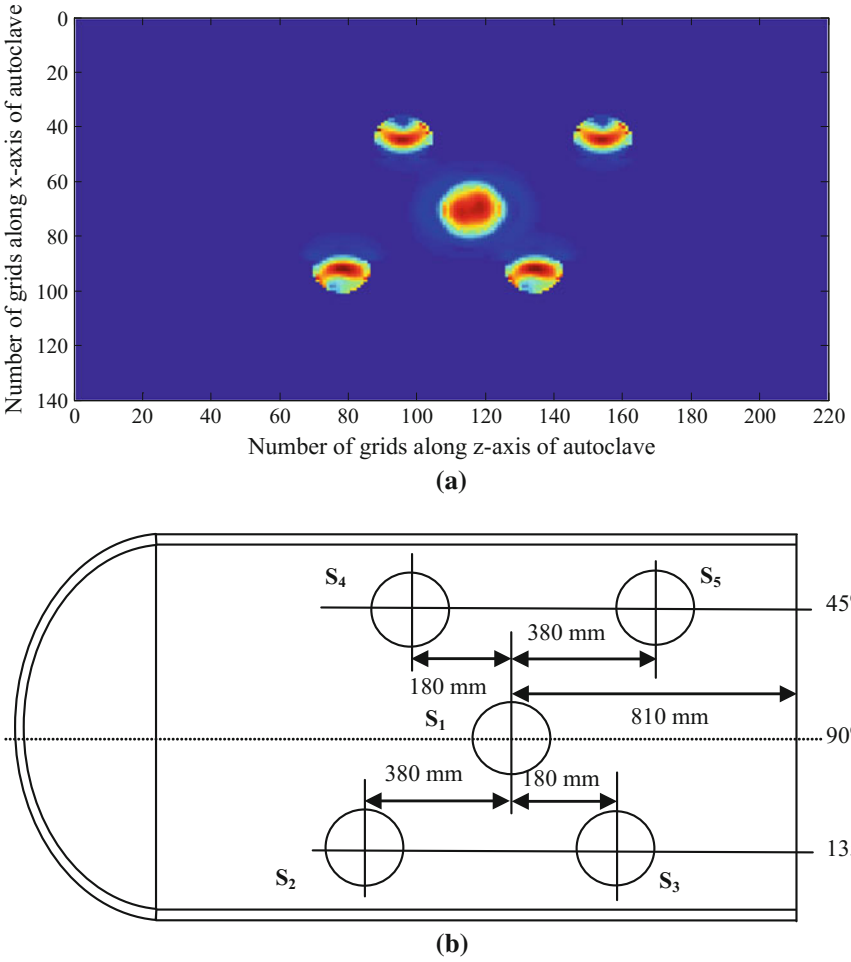

Fig. 56 **a** FDTD modeling of five magnetron source locations with respect to scaled down (1:2) autoclave geometry. **b** *Top view* of actual hybrid-cylindrical autoclave excited with five sources

cross section at all cuts. Although the strength of the field is not uniform across the circular cross section of autoclave, the field seems to be uniform near to the metallic table. Further, the electric field distribution inside cavity is estimated in *yz*-plane at different cuts along *x*-axis measured from left to right side of the autoclave as shown in Figs. 66, 67, 68, 69, 70, 71, 72, 73, 74, and 75. It is observed that the field distributions are very weak in *yz*-plane at the extreme left and right cuts. The intensity of field distribution in *yz*-plane increases as plane moves to the center of the autoclave from left to right side.

Finally, the electric field distribution inside the autoclave cavity is determined in *zx*-plane at different cuts along *y*-axis measured from top to the bottom of the

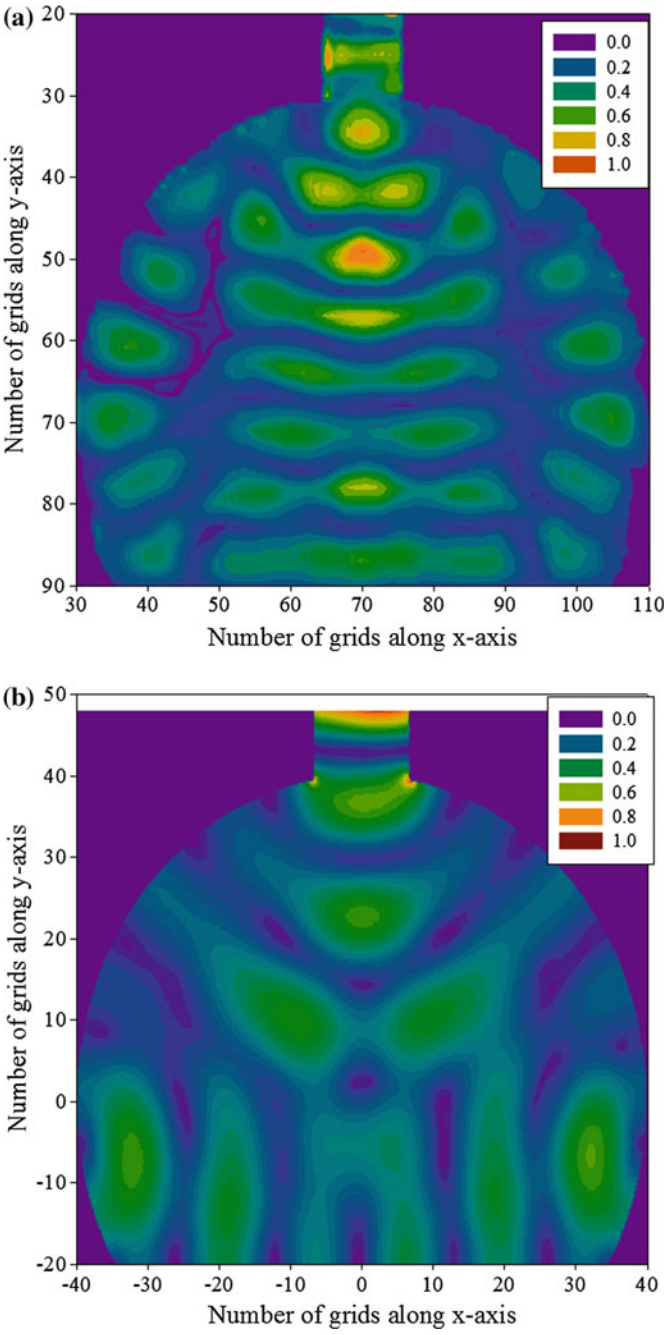

Fig. 57 Normalized total electric field (magnitude) distribution inside the autoclave cavity excited with single source in *xy*-plane at z = 70th grid (middle point of cavity length) computed based on: **a** proposed FDTD method, and **b** software package

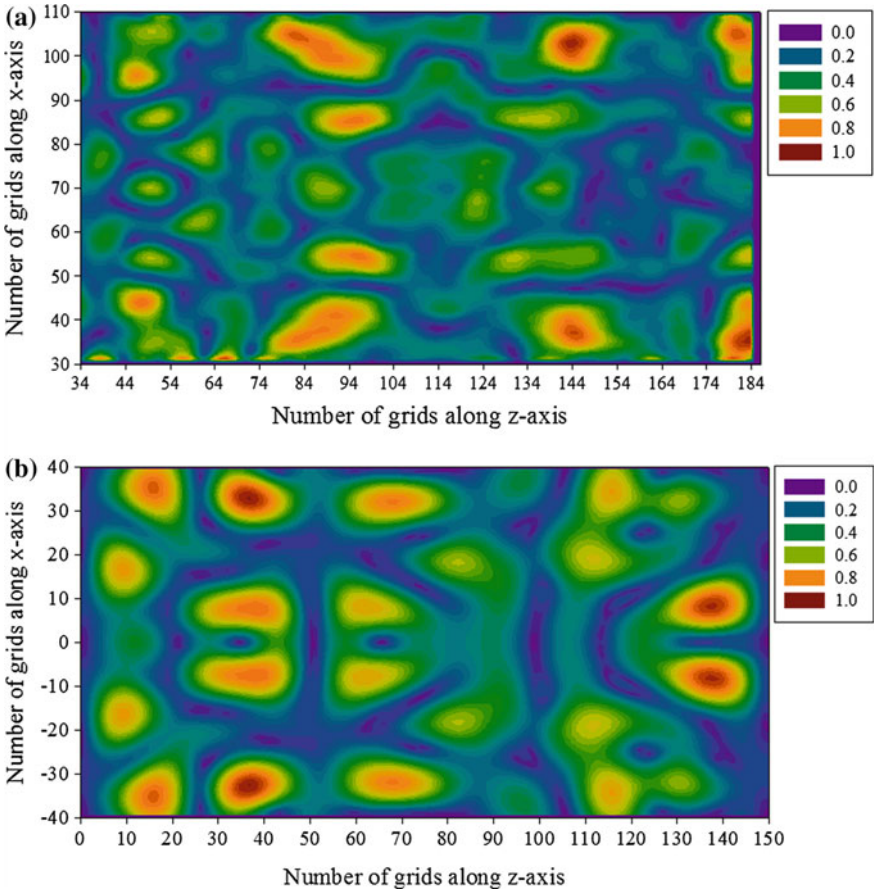

Fig. 58 Normalized total electric field (magnitude) distribution inside the autoclave cavity excited with single source in *zx*-plane at y = 14th grid (from the metallic plate) computed based on: **a** proposed FDTD method, and **b** software package

autoclave as shown in Figs. 76, 77, 78, 79, 80, 81, 82, 83, 84, 85, 86, 87, 88, 89, and 90. It is observed that the intensity of field distribution increases in *zx*-plane as we move from top to the bottom. Moreover, the field distributions become uniform in *zx*-plane near to the metallic plate. It is evident from the Figs. 88, 89, and 90. It may to be noted that electric field in the above-mentioned planes is computed in the unit of V/m and then normalized with regard to the maximum field value in that plane.

To summarize, the electric field inside the autoclave is more properly distributed due to the five sources as compared to single source. Further in the case of five sources, the field distribution is found to be more uniform and intense in *zx*-plane near to the metallic plate as compared to that of other planes. Finally, it is concluded that with the current positions of the five sources on the autoclave, uniform field

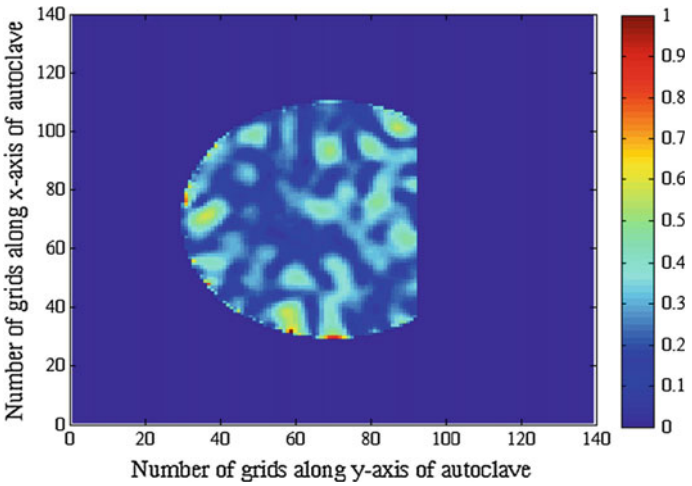

Fig. 59 Normalized total electric field (magnitude) distribution inside the hybrid-cylindrical autoclave in *xy*-plane at z = 190 mm

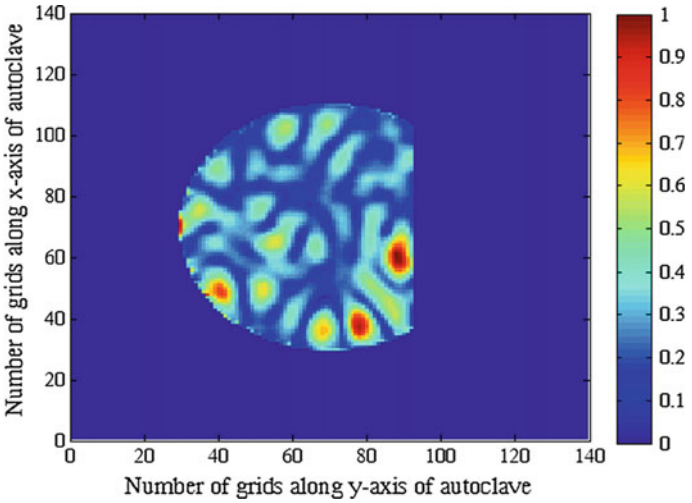

Fig. 60 Normalized total electric field (magnitude) distribution inside the hybrid-cylindrical autoclave in *xy*-plane at z = 290 mm

distributions can be achieved near to the metallic plate in all planes for curing the material loaded on the turntable. This can be confirmed by keeping a sample inside the autoclave cavity, which is discussed in detail as follows.

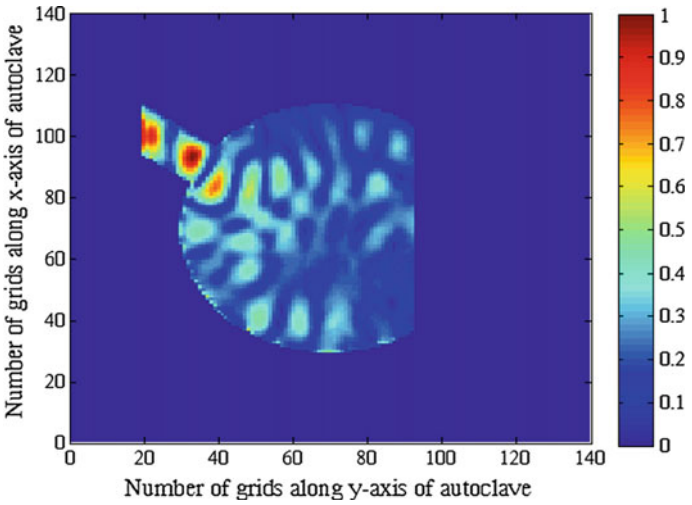

Fig. 61 Normalized total electric field (magnitude) distribution inside the hybrid-cylindrical autoclave in *xy*-plane at z = 390 mm

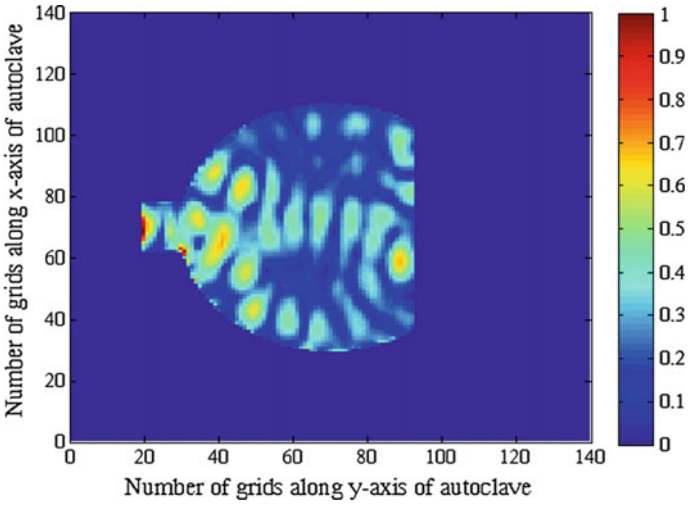

Fig. 62 Normalized total electric field (magnitude) distribution inside the hybrid-cylindrical autoclave in *xy*-plane at z = 590 mm

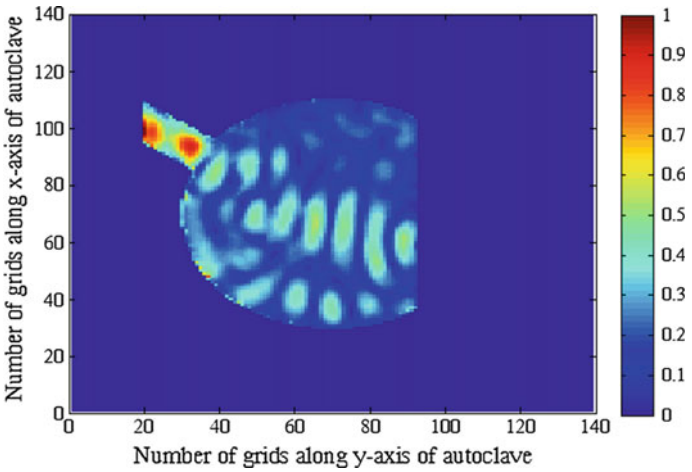

Fig. 63 Normalized total electric field (magnitude) distribution inside the hybrid-cylindrical autoclave in *xy*-plane at z = 690 mm

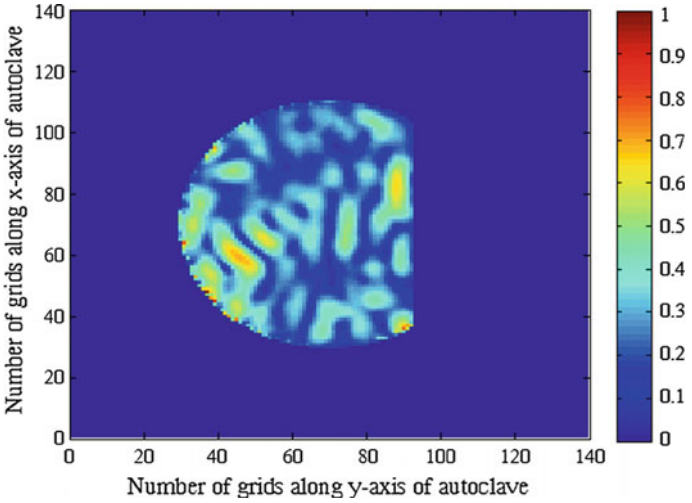

Fig. 64 Normalized total electric field (magnitude) distribution inside the hybrid-cylindrical autoclave in *xy*-plane at *z* = 890 mm

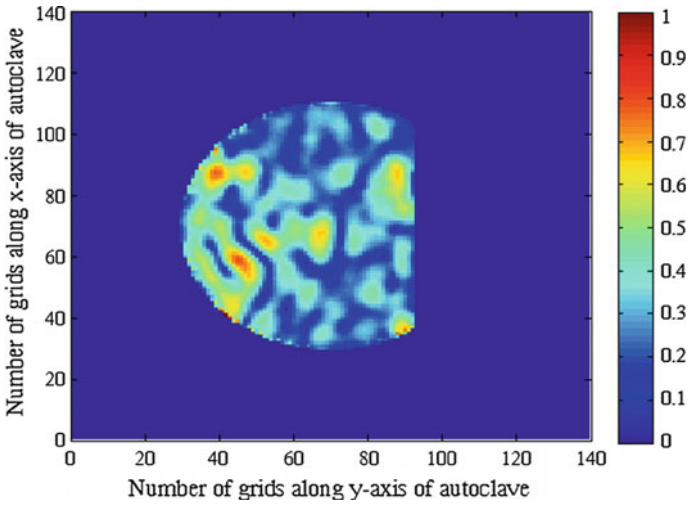

Fig. 65 Normalized total electric field (magnitude) distribution inside the hybrid-cylindrical autoclave in *xy*-plane at $z = 910$ mm

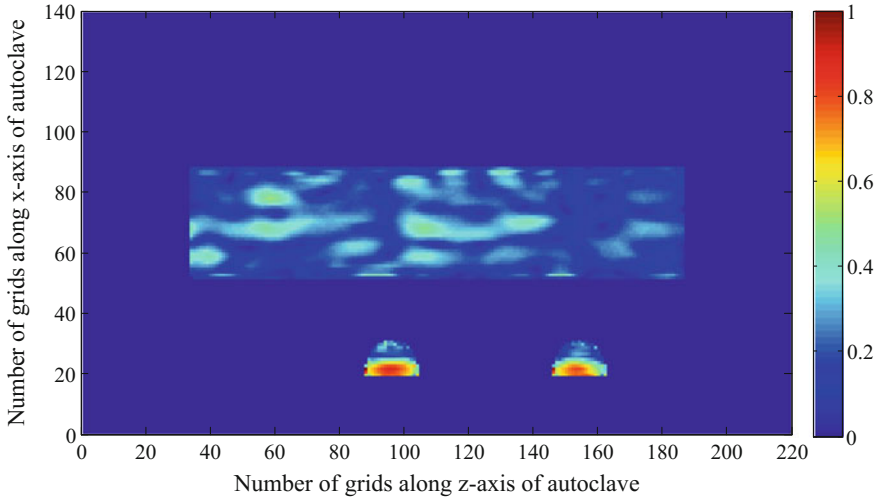

Fig. 66 Normalized total electric field (magnitude) distribution inside the hybrid-cylindrical autoclave in *yz*-plane at $x = 170$ mm

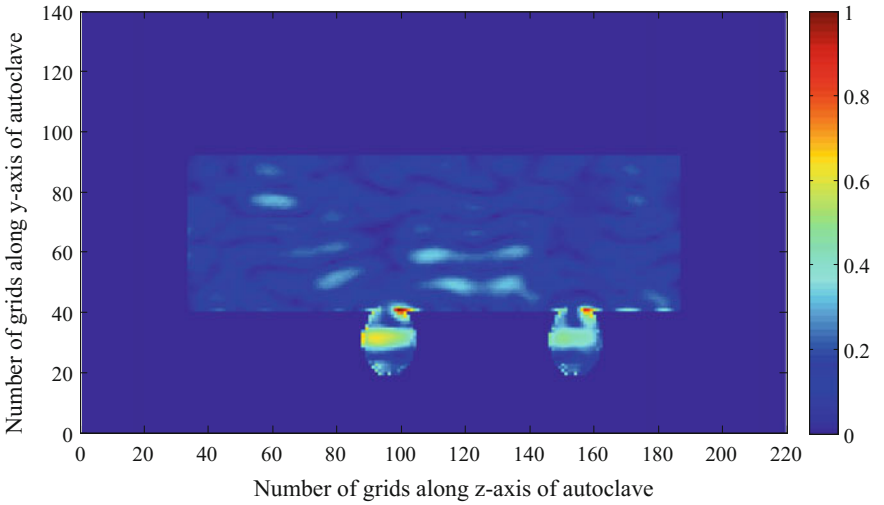

Fig. 67 Normalized total electric field (magnitude) distribution inside the hybrid-cylindrical autoclave in *yz*-plane at $x = 210$ mm

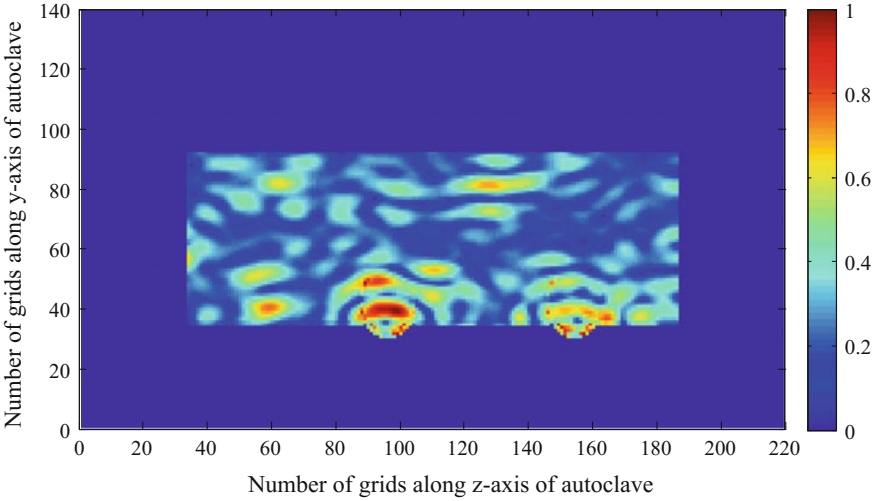

Fig. 68 Normalized total electric field (magnitude) distribution inside the hybrid-cylindrical autoclave in *yz*-plane at $x = 250$ mm

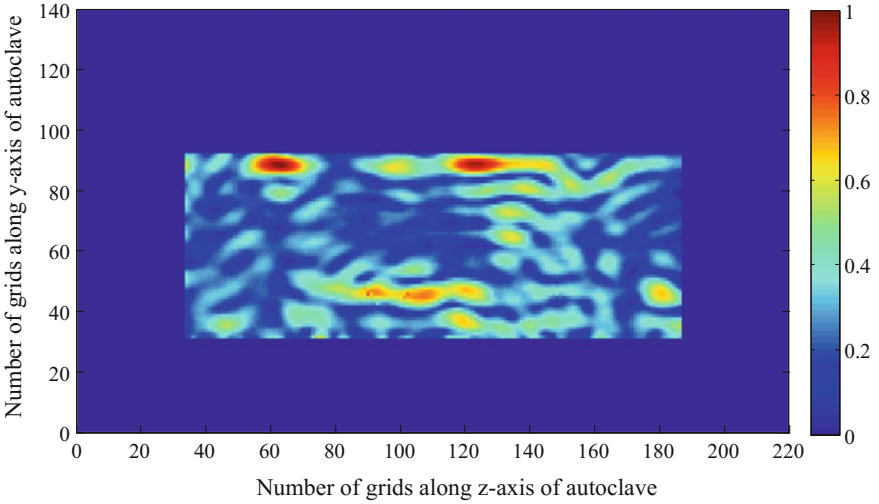

Fig. 69 Normalized total electric field (magnitude) distribution inside the hybrid-cylindrical autoclave in *yz*-plane at x = 290 mm

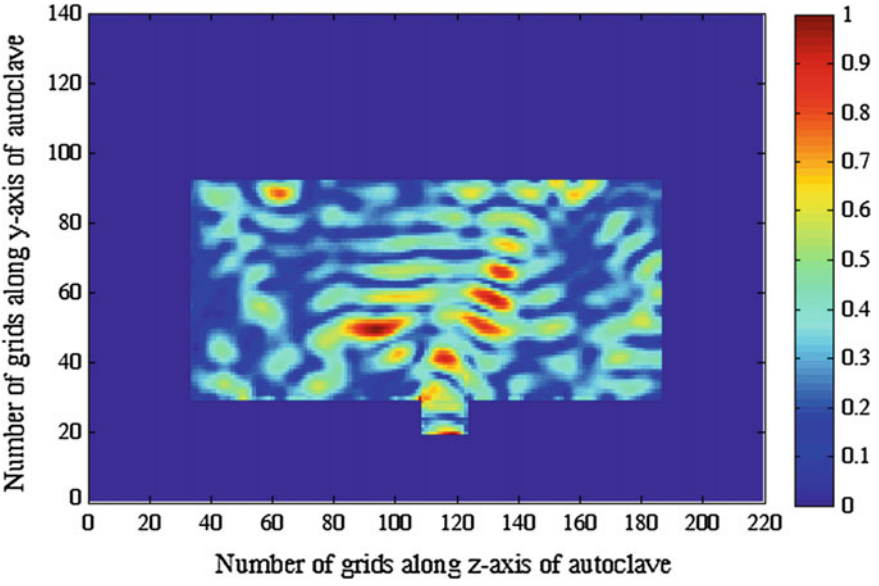

Fig. 70 Normalized total electric field (magnitude) distribution inside the hybrid-cylindrical autoclave in *yz*-plane at x = 330 mm

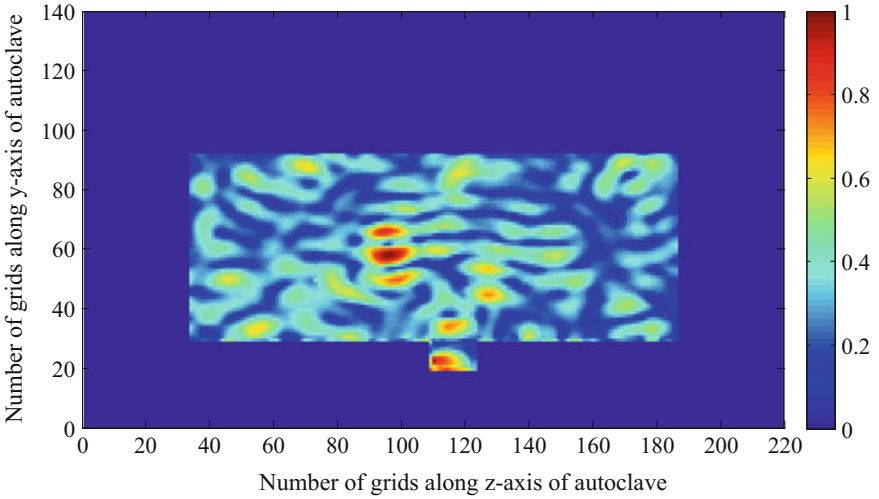

Fig. 71 Normalized total electric field (magnitude) distribution inside the cylindrical autoclave in *yz*-plane at $x = 370$ mm

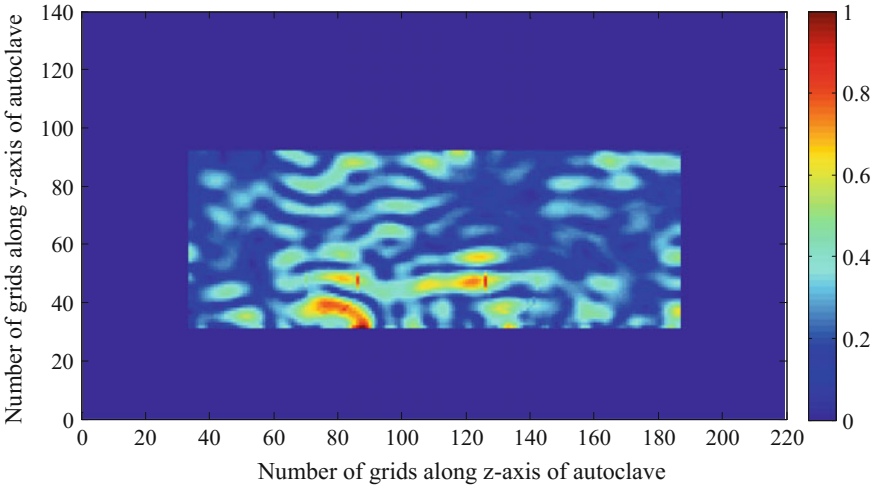

Fig. 72 Normalized total electric field (magnitude) distribution inside the hybrid-cylindrical autoclave in *yz*-plane at $x = 410$ mm

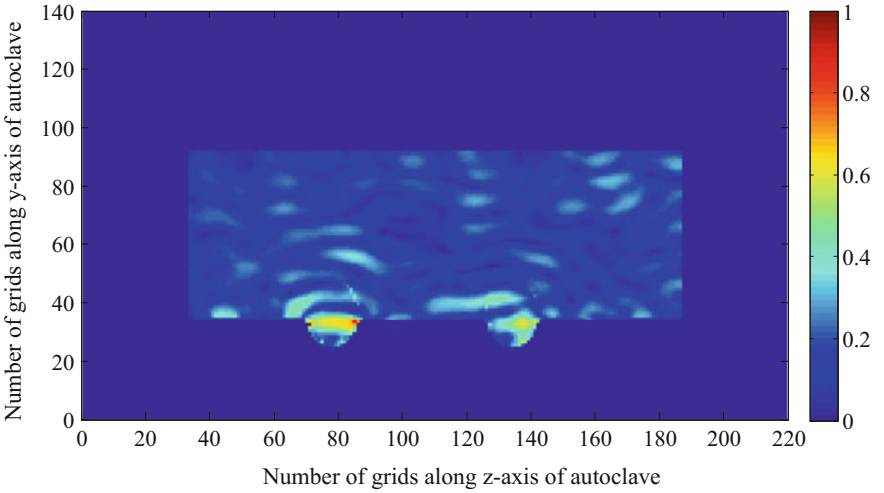

Fig. 73 Normalized total electric field (magnitude) distribution inside the hybrid-cylindrical autoclave in *yz*-plane at x = 450 mm

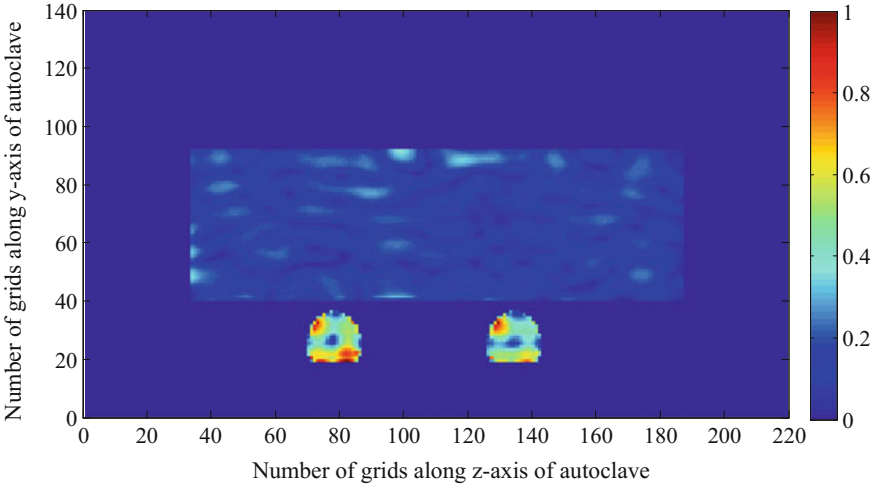

Fig. 74 Normalized total electric field (magnitude) distribution inside the hybrid-cylindrical autoclave in *yz*-plane at x = 490 mm

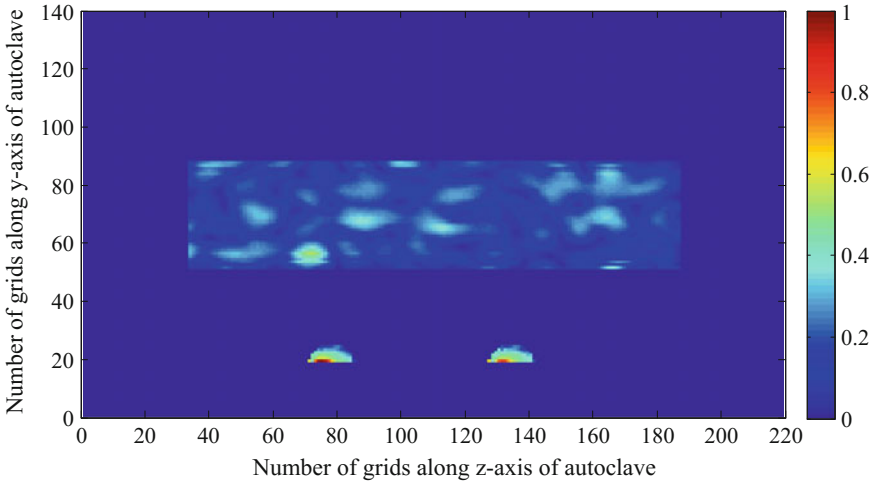

Fig. 75 Normalized total electric field (magnitude) distribution inside the hybrid-cylindrical autoclave in *yz*-plane at x = 530 mm

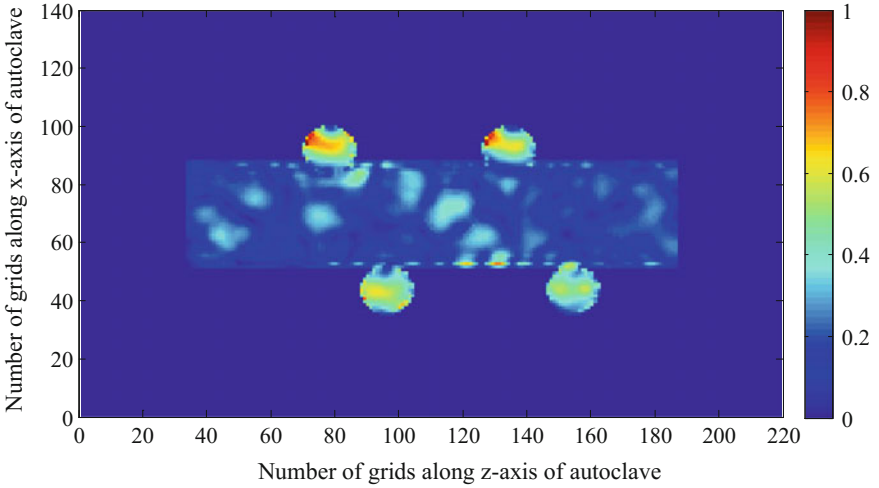

Fig. 76 Normalized total electric field (magnitude) distribution inside the hybrid-cylindrical autoclave in *zx*-plane at y = 170 mm

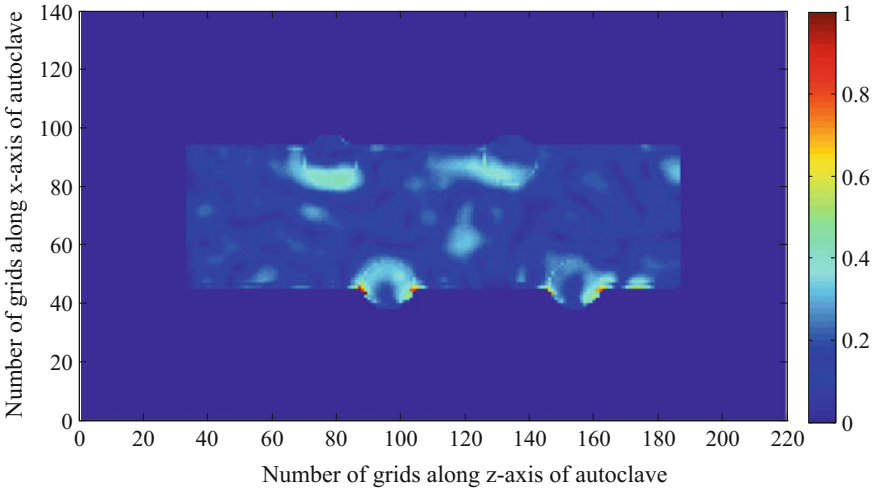

Fig. 77 Normalized total electric field (magnitude) distribution inside the hybrid-cylindrical autoclave in *zx*-plane at y = 190 mm

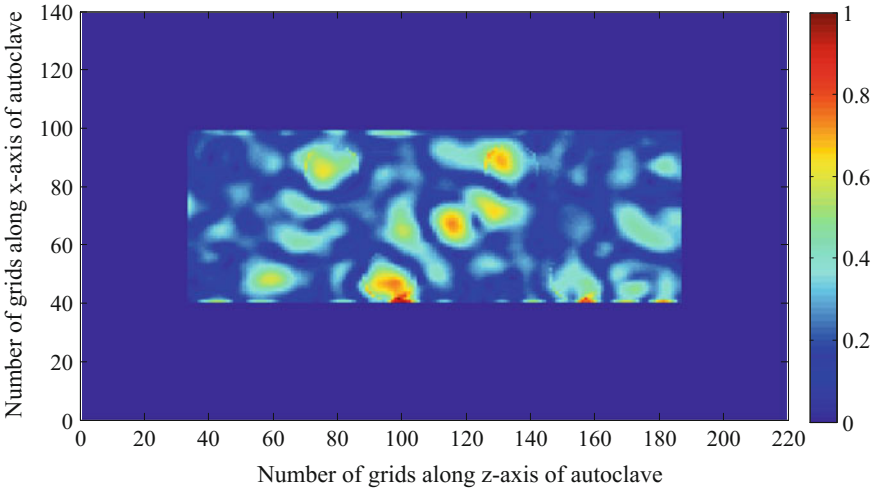

Fig. 78 Normalized total electric field (magnitude) distribution inside the hybrid-cylindrical autoclave in *zx*-plane at y = 210 mm

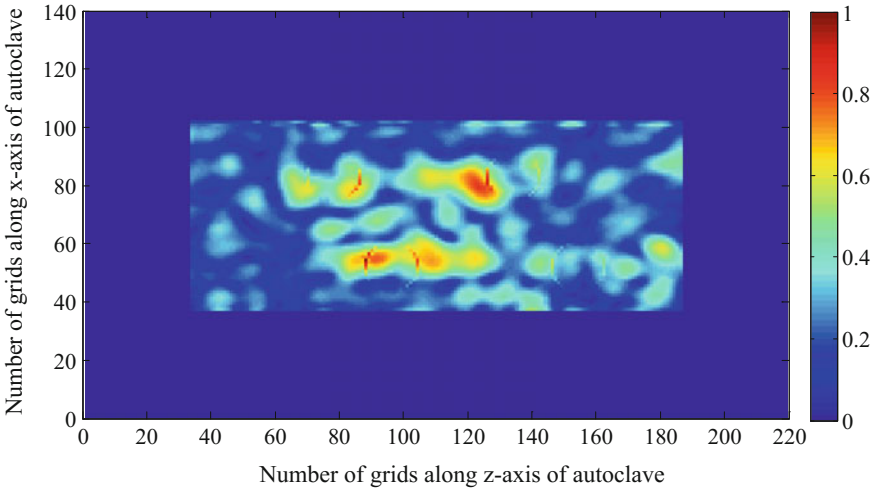

Fig. 79 Normalized total electric field (magnitude) distribution inside the hybrid-cylindrical autoclave in *zx*-plane at y = 230 mm

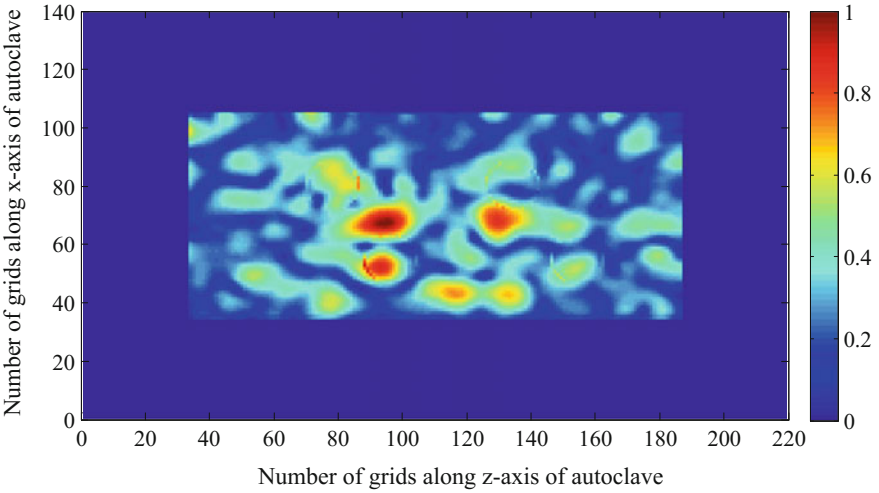

Fig. 80 Normalized total electric field (magnitude) distribution inside the hybrid-cylindrical autoclave in *zx*-plane at y = 250 mm

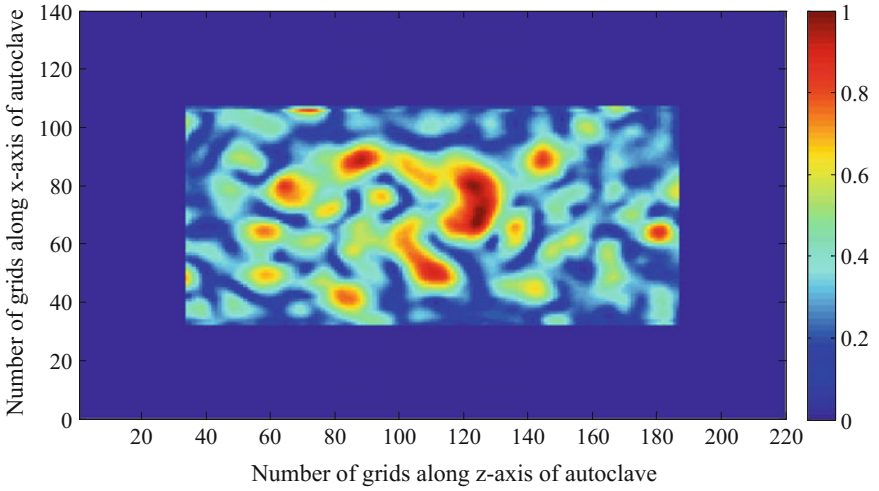

Fig. 81 Normalized total electric field (magnitude) distribution inside the hybrid-cylindrical autoclave in *zx*-plane at y = 260 mm

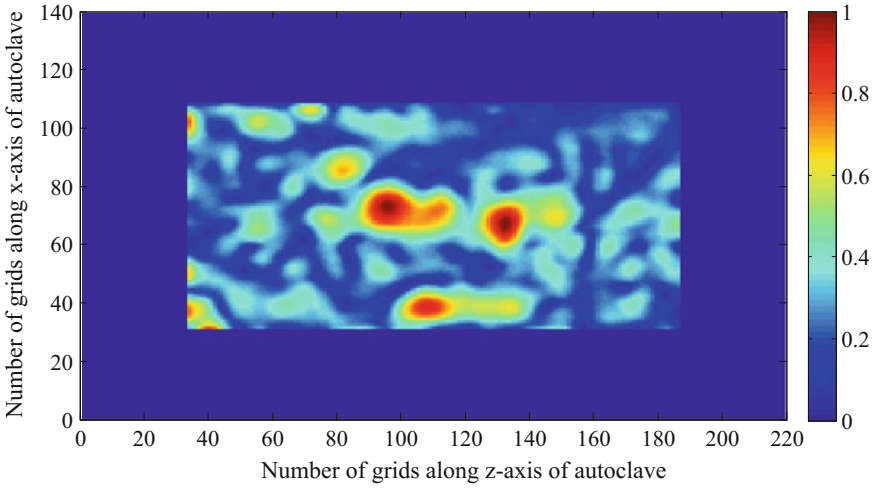

Fig. 82 Normalized total electric field (magnitude) distribution inside the hybrid-cylindrical autoclave in *zx*-plane at y = 290 mm

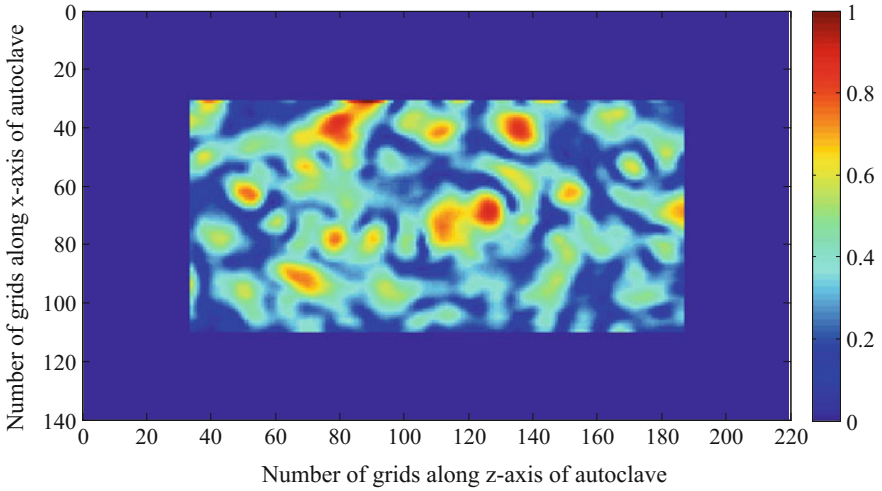

Fig. 83 Normalized total electric field (magnitude) distribution inside the hybrid-cylindrical autoclave in *zx*-plane at $y = 310$ mm

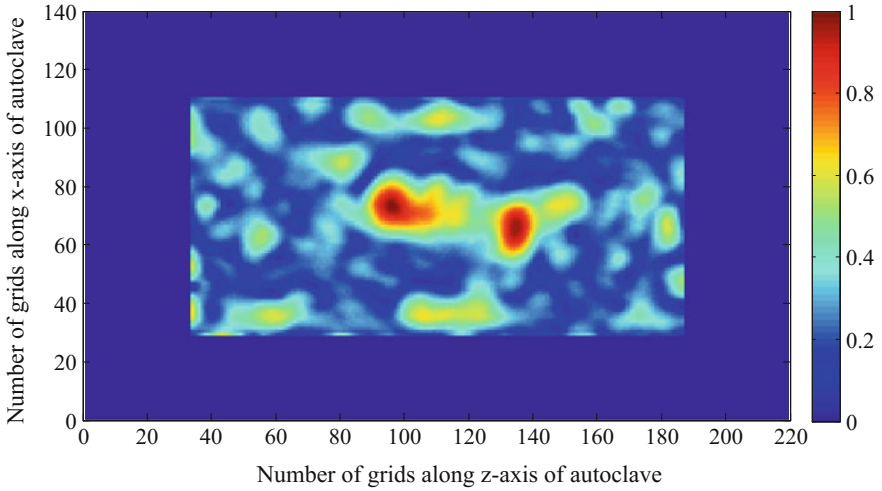

Fig. 84 Normalized total electric field (magnitude) distribution inside the hybrid-cylindrical autoclave in *zx*-plane at $y = 330$ mm

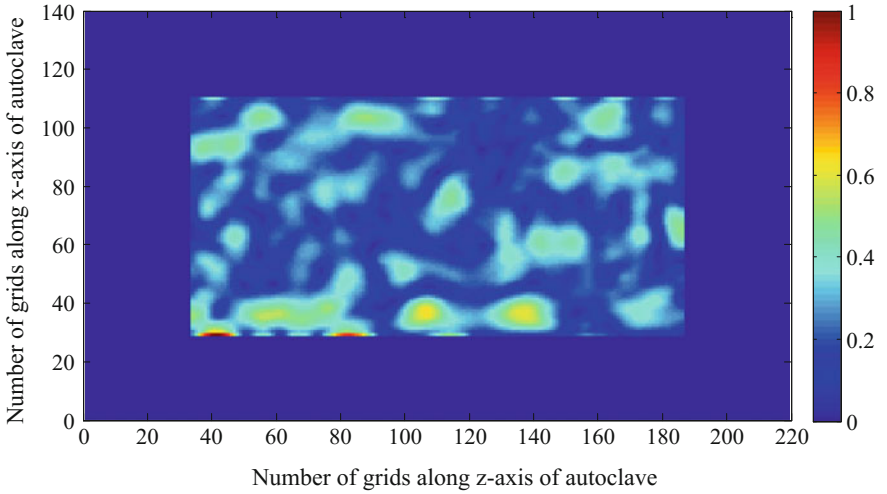

Fig. 85 Normalized total electric field (magnitude) distribution inside the hybrid-cylindrical autoclave in *zx*-plane at y = 350 mm

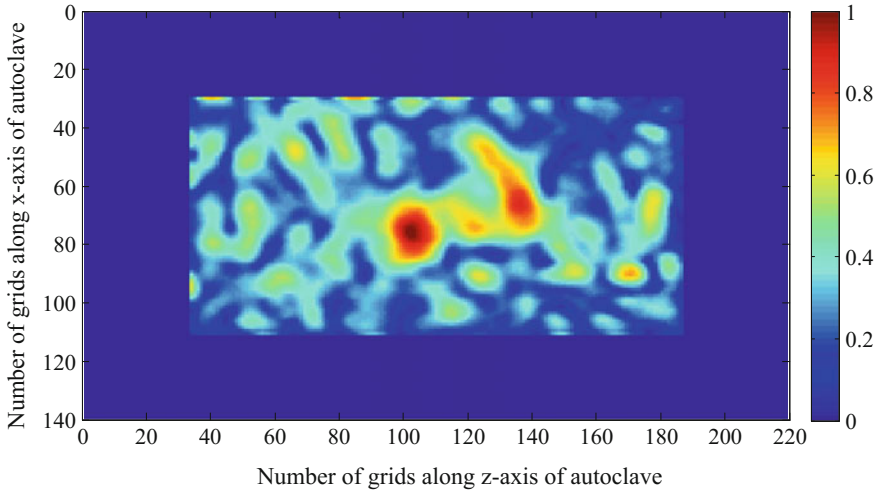

Fig. 86 Normalized total electric field (magnitude) distribution inside the hybrid-cylindrical autoclave in *zx*-plane at y = 370 mm

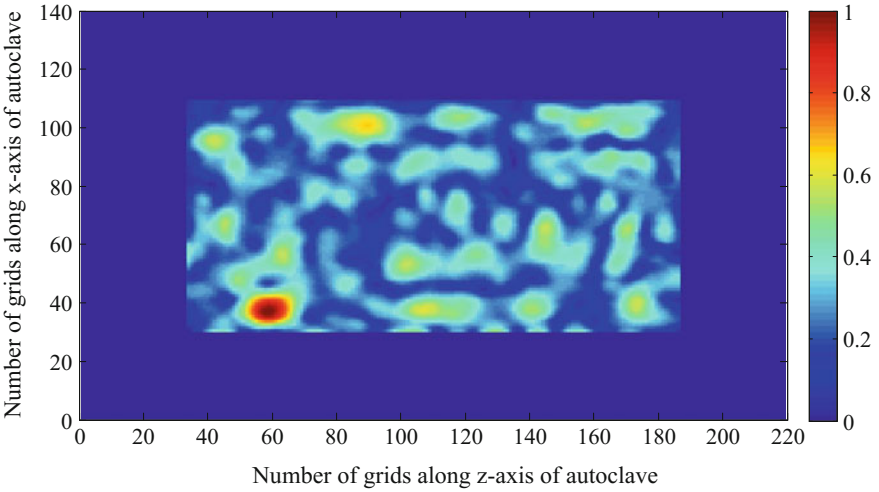

Fig. 87 Normalized total electric field (magnitude) distribution inside the hybrid-cylindrical autoclave in *zx*-plane at y = 390 mm

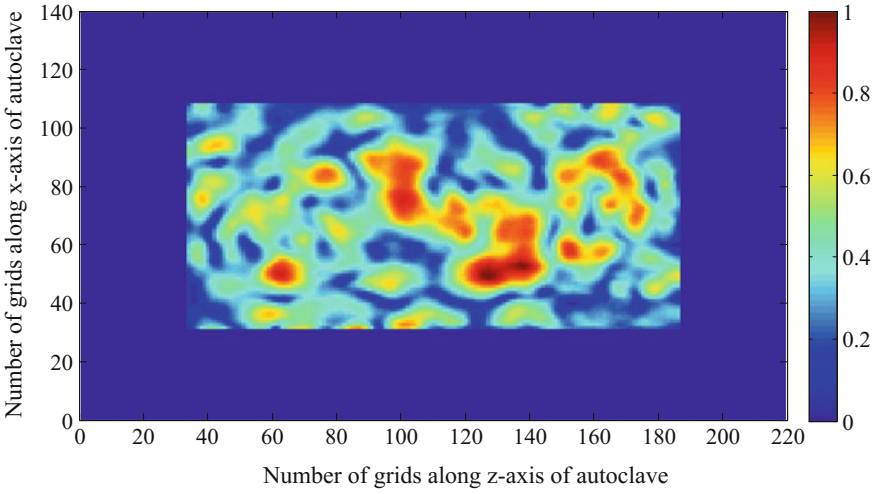

Fig. 88 Normalized total electric field (magnitude) distribution inside the hybrid-cylindrical autoclave in *zx*-plane at y = 410 mm

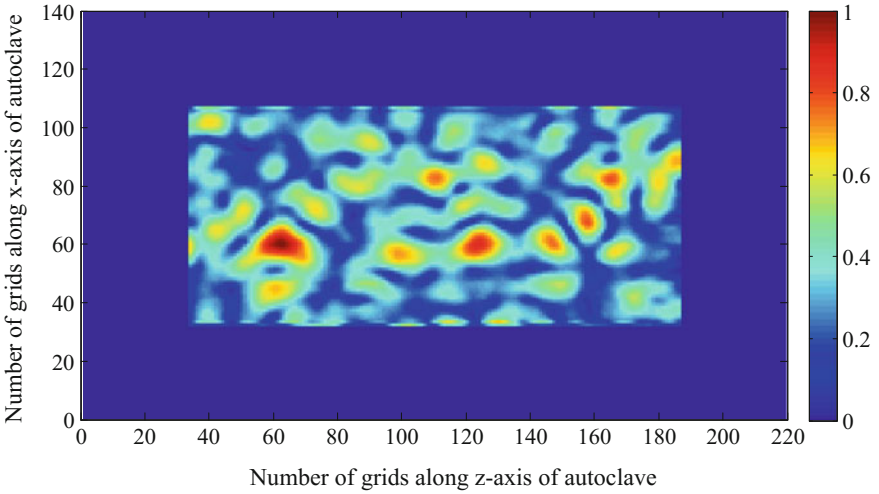

Fig. 89 Normalized total electric field (magnitude) distribution inside the hybrid-cylindrical autoclave in *zx*-plane at y = 430 mm

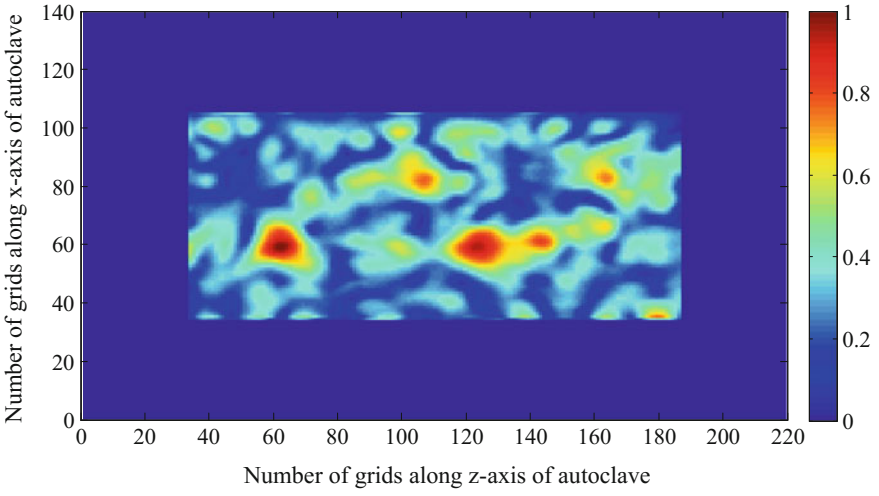

Fig. 90 Normalized total electric field (magnitude) distribution inside the hybrid-cylindrical autoclave in *zx*-plane at y = 450 mm

4.2.3 EM Field Distribution Inside the Autoclave Cavity in the Presence of Sample

In order to show the usability of the proposed autoclave (i.e., with five magnetron sources) for curing the aerospace materials/components, a cylindrical sample of

typical E-glass epoxy (ε_r = 4.0 and tan δ_e = 0.015) is kept at the middle portion of the metallic table in a such way that the center of the cylinder axis located inside the autoclave cavity at point (70th, 82nd, and 110th). The length and diameter of the cylindrical sample are considered to be 300 and 100 mm, respectively. The field distribution inside autoclave cavity is estimated in *xy*-, *yz*-, and *zx*-planes in the presence of cylindrical sample. Figures 91, 92, and 93 represent the electric field inside the autoclave in *xy*-plane in the presence of sample, where encircled portion shows the field distribution across the cylindrical sample. It is observed that the field distribution across circular cross section of the sample is uniform corresponding to different cuts along *z*-axis.

Further electric field distribution is estimated inside autoclave cavity in *yz*-plane in the presence of cylindrical sample at different cuts along *x*-axis, i.e., x = 325, 350, and 375 mm, which are shown in Figs. 94, 95, and 96, respectively. The field distribution is observed to be uniform across the sample in *yz*-plane for different cuts along *x*-axis. Finally, field distribution across cylindrical sample is studied in *zx*-plane for different cuts along *y*-axis (Figs. 97, 98 and 99). The field distribution across the sample is observed to be uniform in *zx*-plane corresponding to different cuts along *y*-axis. Thus, the hybrid-cylindrical autoclave excited with five sources is capable of curing aerospace materials and components especially more suitable for UAV's (unmanned air vehicles) and MAV's components and materials.

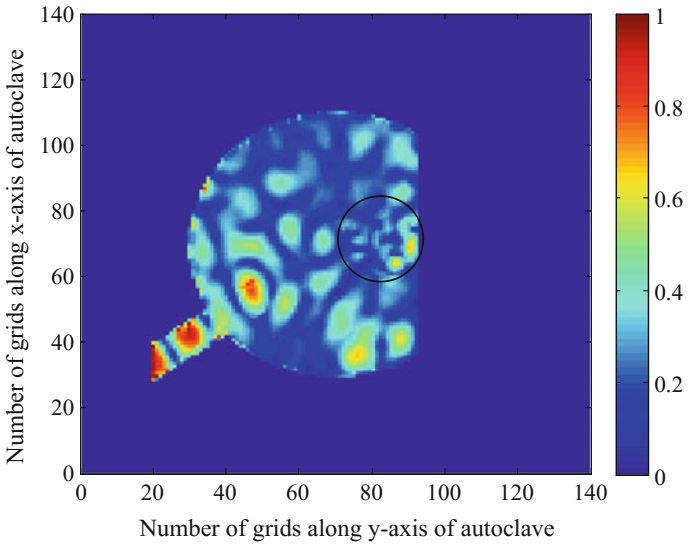

Fig. 91 Normalized total electric field (magnitude) distribution inside the autoclave cavity in the presence of cylindrical sample in *xy*-plane at z = 450 mm (sample region is *encircled* in the graph)

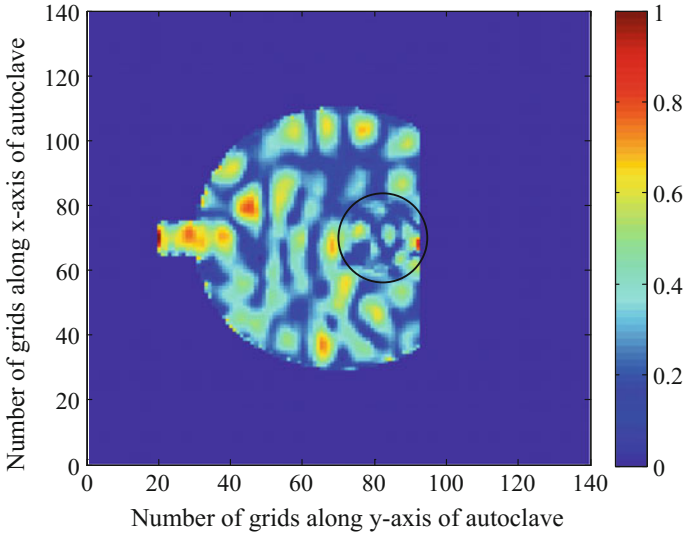

Fig. 92 Normalized total electric field (magnitude) distribution inside the autoclave in the presence of cylindrical sample in *xy*-plane at z = 550 mm (sample region is *encircled* in the graph)

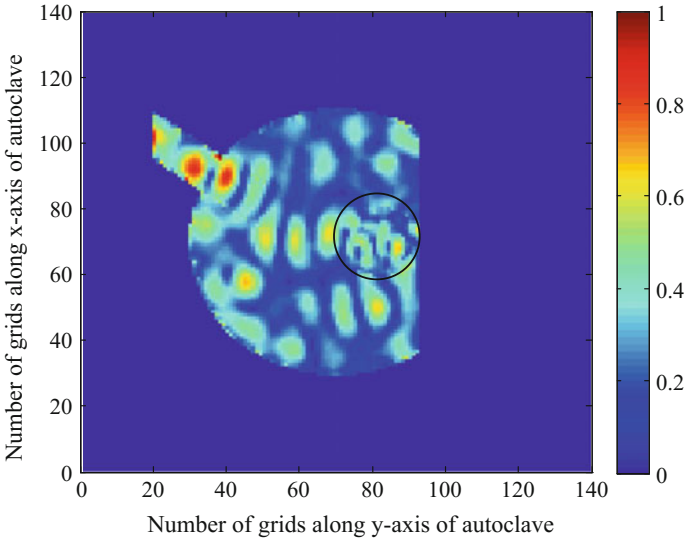

Fig. 93 Normalized total electric field (magnitude) distribution inside the autoclave in the presence of cylindrical sample in *xy*-plane at z = 650 mm

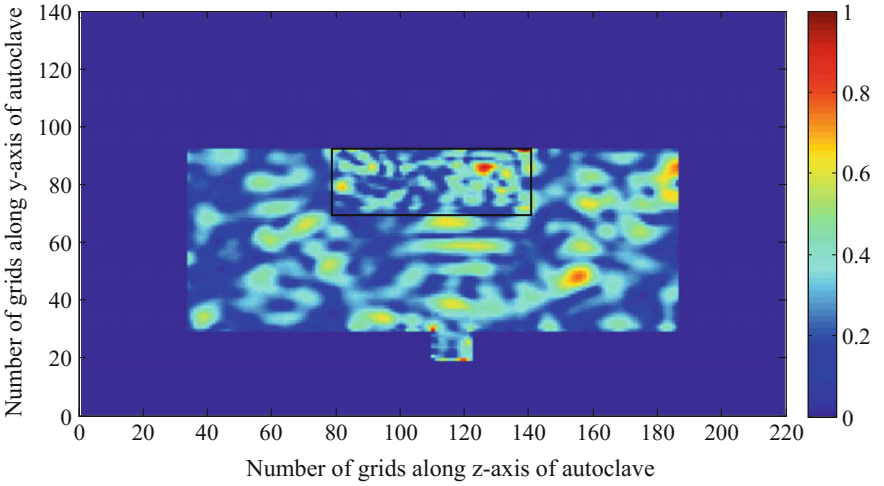

Fig. 94 Normalized total electric field (magnitude) distribution inside the autoclave in the presence of cylindrical sample in *yz*-plane at $x = 325$ mm (sample region is *encircled* in the graph)

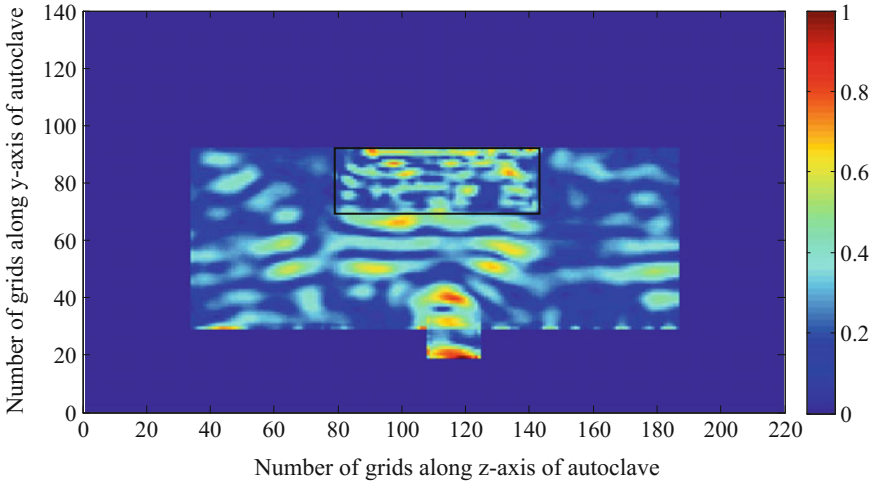

Fig. 95 Normalized total electric field (magnitude) distribution inside the autoclave in the presence of cylindrical sample in *yz*-plane at $x = 350$ mm (sample region is *encircled* in the graph)

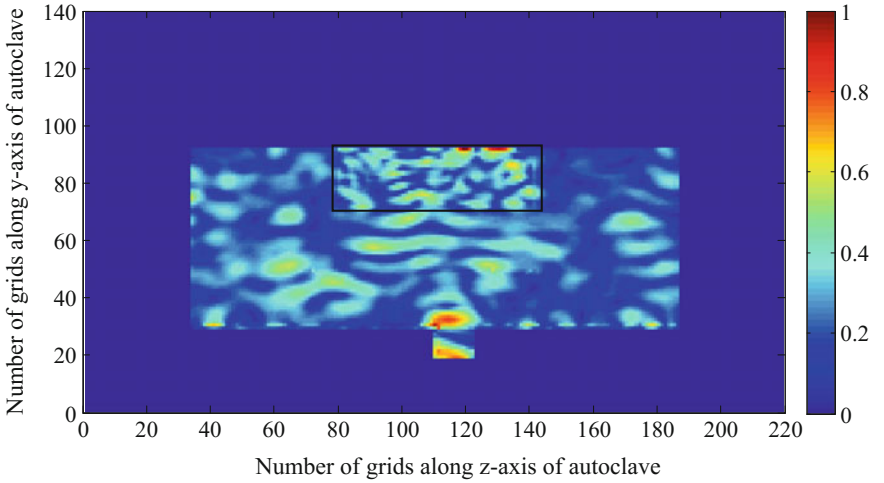

Fig. 96 Normalized total electric field (magnitude) distribution inside the autoclave in the presence of cylindrical sample in *yz*-plane at $x = 375$ mm (sample region is *encircled* in the graph)

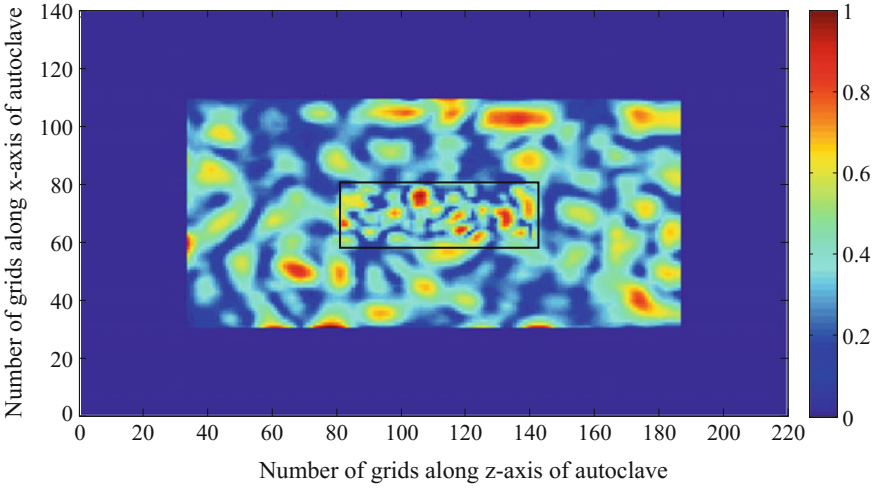

Fig. 97 Normalized total electric field (magnitude) distribution inside the autoclave in the presence of cylindrical sample in *zx*-plane at $y = 385$ mm (sample region is *encircled* in the graph)

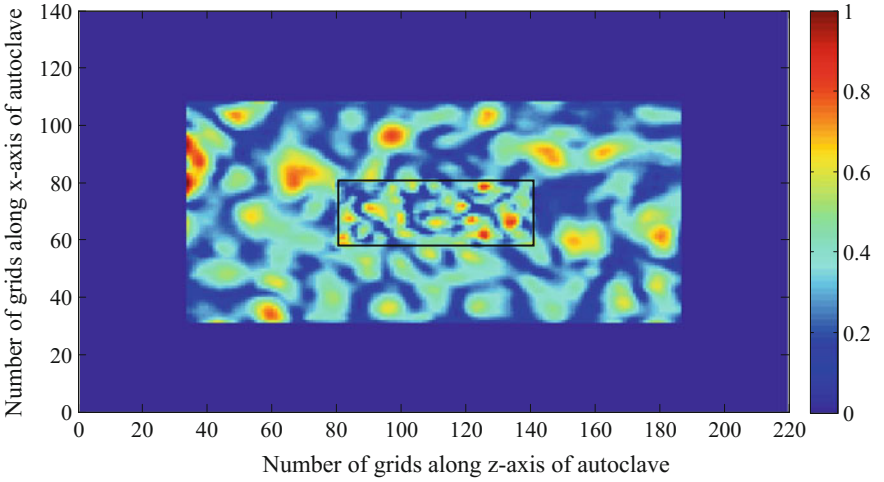

Fig. 98 Normalized total electric field (magnitude) distribution inside the autoclave in the presence of cylindrical sample in *zx*-plane at $y = 410$ mm (sample region is *encircled* in the graph)

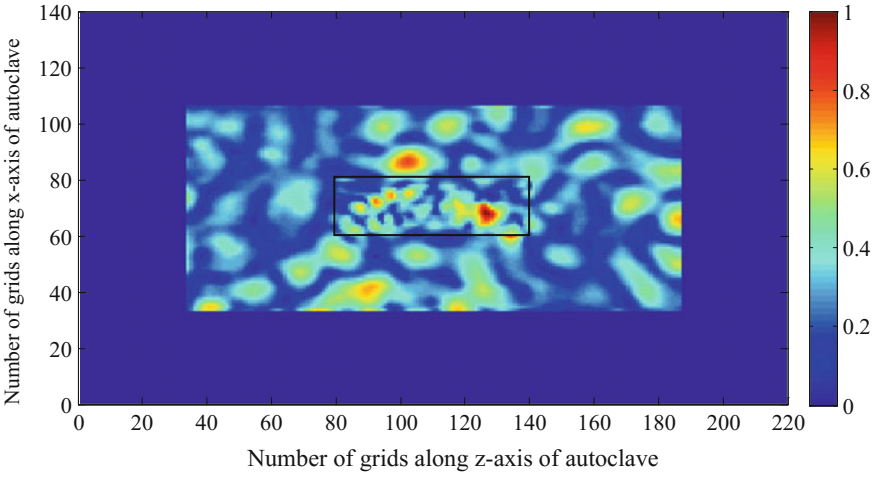

Fig. 99 Normalized total electric field (magnitude) distribution inside the autoclave in the presence of cylindrical sample in *zx*-plane at $y = 435$ mm (sample region is *encircled* in the graph)

5 Summary

This book dealt with the EM analysis of closed microwave cavities based on the three-dimensional FDTD method. The EM analysis is carried out for: (i) rectangular microwave oven and (ii) hybrid-cylindrical microwave autoclave at 2.45 GHz. The field distribution is first estimated inside the domestic rectangular oven in *xy*-, *yz*-,

and *zx*-planes. In *zx*-plane of cavity, the field distribution is found to be more uniform as compared to other planes. Further, the RF leakage from oven door is determined at 2.45 GHz.

Furthermore, the EM analysis of hybrid-cylindrical autoclave is carried out based on 3D FDTD using staircase approximation. The field distribution inside the autoclave cavity is studied by exciting the autoclave with single and multiple (five) magnetron sources. The field distribution inside the autoclave cavity is found to be more uniform in the case of five sources. In addition, the five magnetron sources are capable of forming almost uniform field distribution within a specific region inside the autoclave cavity (i.e., from 55th grid to 95th grid along *x*-axis, from 60th grid to 92nd grid along *y*-axis, and from 55th grid to 175th grid along *z*-axis) near the metallic table. In order to show the capability of autoclave (excited with five source) for curing the aerospace components and materials, the field distribution inside the autoclave cavity is studied in the presence of cylindrical sample of typical glass epoxy. The field distribution is found to be almost uniform across the sample in all planes. The proposed hybrid-autoclave can also be used to tune the field strength and hence temperature distribution inside the autoclave. This book would help the reader to design and analyze the field distribution inside the arbitrary-shaped microwave cavities such as microwave oven and industrial autoclave.

References

Berenger, J.P.: A perfectly matched layer for the absorption of electromagnetic waves. J. Comput. Phys. **114**, 185–200 (1994)

Dev, S.R.S., Gariepy, Y., Orsat, V., Raghavan, G.S.V.: "FDTD modeling and simulation of microwave heating of in-shell eggs. Prog. Electromagn. Res. M **13**, 229–243 (2010)

Hussein, M., Sebak, A.: Application of the finite-difference time-domain method to the analysis of mobile antennas. IEEE Trans. Veh. Technol. **45**, 417–426 (1996)

Jia, X., Jolly, P.: Simulation of microwave field and power distribution in a cavity by a three-dimensional finite element method. J. Microw. Power Electromagn. Energy. **27**, 11–22 (1992)

Kusama, Y., Hashimoto, O., Makida, M.: Size reduction of the door seal structure of a microwave oven by the FDTD method. Electron. Commun. Jpn **86**, 73–83 (2003)

Liao, S.Y.: Microwave Devices and Circuits. Prentice-Hall Int., ISBN-81-203-0699-6, 542 p. (1995)

Pourcq, M.D.: Field and power-density calculations in closed microwave systems by three-dimensional finite difference. In: IEE Proceedings, vol. 132, Pt. H, no. 6, pp. 360–368, Oct. 1985

Rao, S.M.: Time Domain Electromagnetics. Academic press, ISBN 0-12-580190-4, pp. 151–152 (1999)

Samuel, A.C.: Microwave Autoclave Apparatus, US Patent US5436432 A, July 1995

Schneider, J.B.: Understanding the Finite-Difference Time-Domain Method. www.eecs.wsu.edu/~schneidj/ufdtd (2010)

Sullivan, D.M.: Electromagnetic Simulation using the FDTD Method. IEEE Press, 2000

Taflove, A., Browdwin, M.E.: Numerical solution of steady-state electromagnetic scattering problems using the time-dependent Maxwell's equation. IEEE Trans. Microw. Theory Tech. **23**(8), 623–630 (1975)

Taflove, A., Hagness, S.C.: Computational Electrodynamics: The Finite-Difference Time-Domain Method. Artech House, Boston, ISBN 1-58053-076-1, 1038 p. (2005)

Watanabe, M., Suzuki, M., Ohkawa, S.: Analysis of power density distribution in microwave ovens. J. Microw. Power **13**(2), 173–181 (1978)

Yee, K.S.: Numerical solution of initial boundary value problems involving Maxwell's equations in isotropic media. IEEE Trans. Antennas Propag. **17**, 585–589 (1966)

Author Index

S. Narayan et al., *FDTD Modeling of EM Field Inside Microwave Cavities*,
SpringerBriefs in Computational Electromagnetics,
DOI 10.1007/978-981-10-3415-2

Subject Index

S. Narayan et al., *FDTD Modeling of EM Field Inside Microwave Cavities*,
SpringerBriefs in Computational Electromagnetics,
DOI 10.1007/978-981-10-3415-2

Authors Biography

Dr. Shiv Narayan is with the Centre for Electromagnetics of CSIR-National Aerospace Laboratories (CSIR-NAL), Bangalore, India, as Scientist, since 2008. He received Ph.D. degree in Electronics Engineering from Indian Institute of Technology, Banaras Hindu University (IIT-BHU), Varanasi, India, in 2006. He held the position of Scientist B between 2007 and 2008, at SAMEER (Society for Applied Microwave Electronics Engineering and Research), Kolkata, India. His research interests are broadly in the field of electromagnetics applications; these include frequency selective surfaces (FSS), metamaterials, numerical methods (FDTD and MM-GSM) in electromagnetics, antennas, and EM material characterization. He has published a SpringerBrief on FSS-based high-performance antennas in 2015. Dr Shiv is the author/ co-author of over 40 technical documents including peer-reviewed journal and conference papers.

Ms. K.M. Divya received her B. Tech. degree in Electronics and Communication Engineering from Calicut University, Kerala, in 2010 and completed her M. Tech. degree in Microwave and Radar Electronics from Cochin University of Science and Technology (CUSAT), Kerala, in 2013. She was associated with the Centre for Electromagnetics, CSIR-NAL, as Project Scientist from November 2013 to May 2015. Her research interest includes the topics: FDTD modeling, FSS, and metamaterials.

Mr. V. Krushna Kanth obtained his B.Tech (ECE) degree from Jawaharlal Nehru Technological University (JNTU), Anantapur, Andhra Pradesh, India, in 2012. He obtained his M. Tech. degree in Electronics Engineering from Pondicherry Central University, Pondicherry (UT), in 2015. He is currently a Project Assistant-III with the Centre for Electromagnetics of CSIR-National Aerospace Laboratories (CSIR-NAL), Bangalore, India. His current area of research interest includes FSS, RCS field computation, and FDTD-based modeling.

S. Narayan et al., *FDTD Modeling of EM Field Inside Microwave Cavities*,
SpringerBriefs in Computational Electromagnetics,
DOI 10.1007/978-981-10-3415-2

About the Book

This book deals with the FDTD-based EM modeling of microwave cavities such as microwave oven and hybrid-cylindrical autoclaves. In this endeavor, the EM analysis of field distribution inside a domestic microwave oven is first investigated. Further, the RF leakage radiation from the oven door is studied.

In order to cure the aircraft material and components, a hybrid-cylindrical microwave autoclave is proposed, which is excited with multiple magnetron sources. The EM field distribution inside autoclave is analyzed using three-dimensional FDTD in *xy*-, *yz*-, and *zx*-planes corresponding to different cuts measured along *z*-, *x*-, and *y*-axes, respectively. To assess the capability of proposed autoclave for curing the aircraft materials and components, the EM analysis of field distribution inside autoclave cavity is studied in the presence of composite materials of different shapes.

The FDTD-based modeling of microwave oven and autoclave is explained herewith the appropriate expressions and illustrations. It is expected that this book would definitely help the readers to design and analyze the arbitrary-shaped microwave cavities such as microwave oven and industrial autoclave.

S. Narayan et al., *FDTD Modeling of EM Field Inside Microwave Cavities*,
SpringerBriefs in Computational Electromagnetics,
DOI 10.1007/978-981-10-3415-2